

CHAOS IN OPTICAL SYSTEMS

P. SZLACHETKA AND K. GRYGIEL

*Nonlinear Optics Division, Institute of Physics, Adam Mickiewicz University,
Poznań, Poland*

CONTENTS

- I. Introduction
 - A. Chaos in Lasers
 - B. Chaos in Nonlinear Optics
 - II. Chaos in Second-Harmonic Generation of Light
 - A. Introduction
 - B. Basic Equations
 - C. Simplest Case: $\gamma_i = 0, \Delta_i = 0, f_i = 0$
 - D. Coherent External Field
 - E. Modulated External Field
 - F. Pulsed External Field
 - G. Final Remarks
 - III. Chaos in Kerr Oscillators
 - A. Introduction
 - B. Basic Equations
 - C. Dynamics of Linearly Coupled Kerr Oscillators
 - 1. Noninteracting Oscillators
 - 2. Interacting Oscillators
 - 3. Synchronization
 - 4. Chaotic Beats
 - 5. Final Remarks
 - D. Dynamics of Nonlinearly Coupled Kerr Oscillators
 - 1. Noninteracting Oscillators
 - 2. Interacting Oscillators
 - 3. Final Remarks
 - IV. Quantum Chaos
 - A. Chaos in a Kerr Oscillator
 - B. Chaos in Second-Harmonic Generation of Light
 - C. Final Remarks
- References

I. INTRODUCTION

It was assumed that a description of evolution of deterministic systems required a solution of the equations of motion, starting from some initial conditions. Although Poincaré [1] knew that it was not always true, this opinion was common. Since the work of Lorenz [2] in 1963, unpredictability of deterministic systems described by differential nonlinear equations has been discovered in many cases. It has been established that given infinitesimally different initial conditions, the outcomes can be wildly different, even with the simplest equations of motion. This feature means the occurrence of *deterministic chaos*. The literature devoted to this multidisciplinary and rapidly developing discipline of science is huge. There are many excellent textbooks, monographs, and collections of main papers, and we mention only a few [3–8].

In this overview we focus our attention on some problems of *optical chaos*. In many optical effects and devices intrinsic instabilities occur and for over thirty years they have been extensively investigated. The literature on optical chaos is widespread and a few excellent reviews and collections of papers should be recalled [9–13].

After an overview of the main papers devoted to chaos in lasers (Section I.A) and in nonlinear optical processes (Section I.B), we present a more detailed analysis of dynamics in a process of second-harmonic generation of light (Section II) as well as in Kerr oscillators (Section III). The last case we consider particularly in the context of coupled nonlinear systems. Finally, we present a cumulant approach to the problem of quantum corrections to the classical dynamics in second-harmonic generation and Kerr processes (Section IV).

A. Chaos in Lasers

Since the discovery of lasers it has been known that a derivation of time-dependent equations governing interaction of molecules with electromagnetic cavity modes leads to the so-called spontaneous instabilities. These laser instabilities were also observed experimentally — even for the first laser built by Maiman in 1960. A random, periodic, or quasiperiodic train of spikes in a laser generation is a fundamental instability due to nonlinearity of laser equations. A comprehensive review of this specific laser-related topics was published in 1983 [14].

A major development reported in 1964 was the first numerical solution of the laser equations by Buley and Cummings [15]. They predicted the possibility of undamped chaotic oscillations far above a gain threshold in lasers. Precisely, they numerically found “almost random spikes” in systems of equations adopted to a model of a single-mode laser with a bad cavity. Thus optical chaos became a subject soon after the appearance Lorenz’ paper [2].

Real development in the field of chaotic properties of laser action began over 10 years later. In 1975 Haken [16] used the model of a single-mode laser with a *homogeneously broadened line* (HBL) described by the Maxwell–Bloch equations and after some approximations showed the equivalence with an appropriate Lorenz system of equations. The model was extended to a multimode case [17]. For a modulated external field, certain laser systems are described by a driven Van der Pol oscillator, and the existence of chaos was found numerically for these systems [18]. In the case of HBL lasers, a spatial inhomogeneity of pump leading to a coupling of different modes, could give rise to an undamped spiking behavior of lasers. This instability is chaotic and was found numerically in a two-mode laser case [19]. A detuning was also incorporated in this model [20], and the exact equivalence between a bad-cavity laser with a modulated inversion and nonlinear oscillator in the Toda potential driven by an external modulation was presented a few years later [21]. The parameters in HBL lasers for which chaos is expected are highly unreal because of big loss in cavity rates. For a detailed discussion of instabilities in HBL lasers, we refer the reader to a treatise by Milonni et al. [13] and a paper by Harrison and Biswas [22].

The Haken model can be easily extended to the case of a single-mode *inhomogeneously broadened line* (IBL) laser [13]. Numerical investigation of the Maxwell–Bloch equations has been carried out for the case of a Doppler broadening and for different parameter ranges, leading to findings of period doubling and intermittency routes to chaos [23,24]. A phenomenon of metastable chaos was also observed. The Maxwell–Bloch equations with an inhomogeneously broadened line were also studied in the context of mode splitting [13,25], bad-cavity instability conditions [26], ring laser configuration [27], Hopf bifurcations [28], and a period doubling route to chaos [29].

Laser instabilities were *experimentally* investigated in many kinds of lasers (see an overview of early papers [14]), but the first experimental observation of the optical chaos was performed by Arecchi et al. [30] in 1982. They used a stabilized CO₂ laser with modulated cavity loss $\Gamma = \gamma(1 + a\cos\Omega t)$ and by changing the frequency of modulation Ω , they found a few period doubling oscillations of the output intensity, both numerically and experimentally.

A detailed analysis shows that the case of the IBL laser is more convenient in experimental investigations because the value of the threshold gain coefficient needed in a laser setup is much smaller. Some spontaneous instability for this case was first discovered experimentally by Casperson quite early [31] in a low-pressure, electric discharge HeXe laser at 3.51 μm . For a special choice of parameters the laser worked in the regime of the so-called self-pulsing instability. But the first chaotic output from an IBL laser was experimentally shown in 1982 by Weiss and King [32] in a HeNe laser (3.39 μm). A period doubling route to chaos was found. In a HeXe laser, Gioggia and Abraham [33] in 1983 reported a chaotic behavior of a generated signal and confirmed period

doubling and intermittency routes to chaos. Similarly, chaotic emission was observed in a ring cavity laser [34]. For an overview of early papers devoted to IBL laser instabilities and chaos, see the study on self-pulsing and chaos in continuous-wave (cw)-excited lasers by Abraham et al. [35].

To achieve the instability of homogeneous broadened line lasers, a satisfaction of much more difficult conditions is required: large gain and the so-called bad-cavity properties. This special regime for damping constants and mode intensity is fulfilled in the far-infrared lasers [36]. In 1985 Weiss et al. [37,38] experimentally found a period doubling route to chaos in the NH_3 laser. Further experimental investigation of chaotic dynamics in such lasers was reported later [39].

The CO_2 lasers were also investigated in connection with chaotic behavior, and here we mention the most important papers in the field. The chaotic behavior associated with a transverse mode structure in a cw CO_2 laser was observed in 1985 [40]. In the CO_2 laser with elasto-optically modulated cavity length, a period doubling route to chaos was also found [41].

Chaos was also investigated in *solid-state lasers*, and the important role of a pump nonuniformity leading to a chaotic lasing was pointed out [42]. A modulation of pump of a solid-state $\text{NdP}_5\text{O}_{14}$ laser leads to period doubling route to chaos [43]. The same phenomenon was observed in the case of laser diodes with modulated currents [44,45]. Also a chaotic dynamics of outputs in Nd:YAG lasers was also discovered [46–48]. In semiconductor lasers a period doubling route to chaos was found experimentally and theoretically in 1993 [49].

An important technique of *chaos control* [50] was introduced in laser systems in 1992 by Roy et al. [51]. They adopted the so-called occasional proportional feedback method to stabilize limit cycles in a multimode Nd:YAG laser with KTP crystal (doubling the basic frequency), pumped by a diode laser. The CO_2 laser with cavity loss modulation was used to implement the control method of output signals proposed by Pyragas [52] and Bielawski et al. [53]. The experimental investigation of the control scheme based on a “washout spectral filter” has been performed in the chaotic regimes of the CO_2 laser with modulated loss [54] as well as in the CO_2 laser with intensity feedback [55]. In 1998, a control of chaos was demonstrated in Nd-doped laser with modulated loss and pump and nonfeedback methods were adopted [56]. These important methods of stabilization of chaotic systems are related to communication theory. In particular, a synchronization of lasers in chaotic regimes has many potential applications. In 1994 Roy and Thornburg proved experimentally for the first time the possibility of synchronization of chaotic lasers [57], with possible applications in digital communication [58]. The last experiments with chaotic lasers revealed a possibility of transmitting a desired message in a very fast way as well as encoding and decoding information in output lasers signals [59–61].

B. Chaos in Nonlinear Optics

Nonlinear optics is a very convenient area to investigate the phenomenon of deterministic chaos both from theoretical and experimental points of view.

The *Jaynes–Cummings* model describing an ensemble of two-level atoms in a resonant cavity with a single-mode field is a basic paradigm in quantum optics. Numerical calculations of the appropriate Maxwell–Bloch equations have revealed a chaotic behavior of the system in a semiclassical approach when no rotating wave approximation is used [62,63]. In a full quantum-mechanical approach, Graham [17] determined the eigenvalues and eigenstates of the coupled atom-field system by numerical diagonalization, and the basis for a quantum description of chaos was prepared. Later, different aspects of chaos in the Jaynes–Cummings model were investigated in a semiclassical or in a full quantum model [64–68].

A complex dynamical behavior was experimentally and numerically found in a system of spin- $\frac{1}{2}$ atoms in an optical resonator with near-resonant cw laser light and external static magnetic field [69]. Three-dimensional Bloch equations were solved, and a chaotic motions was found and compared with experiment.

Quite early optical chaos was found in *optical bistability*. In 1979 Ikeda used a ring cavity configuration for an optically bistable system with two-level absorbing atoms [70]. Ikeda constructed an iterated map of a such system and solving it, found the chaotic output of transmitted field strengths. Moreover, by changing the input light intensities, he proved a period doubling route to chaos. Later, chaos was investigated in the case of off-resonant (dispersive) bistability [71–74]. The first experimental observation of chaos in optical bistability system was made in 1981 by Gibbs et al. [75] in an optical device with electronically introduced delay time. Nakatsuka et al. [76] in 1983 observed experimentally the first chaotic generation in the phenomenon of dispersive bistability. Next, experimental and theoretical evidence of chaotic behavior of signals generated in bistable systems was checked by a few groups [77–82].

Second-harmonic generation of light is a nonlinear phenomenon in which chaotic behavior was discovered in 1983 [83] (for details, see Section II). In the *Kerr effect* with an external time-dependent pump, a chaotic output may also occur, which was proved for the first time in 1990 by Milburn [84] (see also Section III).

Many kinds of molecular systems pumped by a strong laser light show chaotic dynamics. Indeed, in a semiclassical model of a *multiphoton excitation* on molecular vibration, chaos was discovered by Ackerhalt et al. [85] and theoretically and numerically investigated in detail [86,87]. Moreover, the equations of motion that describe a rotating molecule in a laser field can exhibit a chaotic behavior and have been applied in the classical case of a rigid-rotator approximation [87,88].

Dynamical instabilities and chaos were discovered in many light scattering processes. For example Milonni et al. in 1983 [89] found a chaotic strange attractor in *stimulated Raman scattering*. They solved numerically the classical coupled wave equations in the case of perfect phase-matching conditions. Next, a period doubling route to chaos was found, and a fractal dimension of the attractor was calculated by Nath and Ray [90]. Chaos in *stimulated Brillouin scattering* was found in 1984 by Candall and Albritton [91]. The dynamics of generated signals in stimulated scattering processes in optical fibers has also been investigated [92].

Another class of good candidates for a study of chaos in nonlinear optics are *wave-mixing processes* in which chaos appears in the propagation of laser light through passive nonlinear media [93]. A chaotic behavior was observed in three-wave mixing [94] and in four-wave mixing [95].

Experimental work and theoretical investigation show an important role of spatial chaos in optical fibers, directional couplers, and generally in all-optical switching devices [96/97].

The problem of *quantum chaos* in optics has been studied in a few areas. For a short review, see Section IV.

II. CHAOS IN SECOND-HARMONIC GENERATION OF LIGHT

A. Introduction

Nonlinear optics deals with physical systems described by Maxwell equations with an nonlinear polarization vector. One of the best known nonlinear optical processes is the second-harmonic generation (SHG) of light. In this section we consider a well-known set of equations describing generation of the second harmonic of light in a medium with second-order nonlinear susceptibility $\chi^{(2)}$. The classical approach of this section is extended to a quantum case in Section IV.

The first experimental evidence of SHG was reported by Franken et al. [98], who focused a ruby laser beam ($\lambda_L = 0.694$ nm) on a quartz crystal and analyzed the two outgoing beams by a standard method (the second-harmonic beam was observed in the UV region $2\lambda_S = 0.347$ nm). This experiment was soon followed by a theoretical analysis by Armstrong et al. [99]. Since then many articles have appeared on the subject (bibliographies are presented in Refs. 100 and 101).

To analyze the dynamics of SHG, we use time-dependent ordinary differential equations. At the beginning, Maxwell's equations governing SHG were studied, and a simple analytical time dependent solutions was found [99]. The classical case of SHG was discussed by Bloembergen [102], and the present-day state in the dynamics of SHG without damping and pumping was clarified

[103]. The same equations, albeit with damping and coherent external driving field, were studied by Drummond et al. [104] as a particular case of sub/second-harmonic generation. They proved that below a critical pump intensity, the system can reach a stable state (field of constant amplitude). However, beyond the critical intensity, the steady state is unstable. They predicted the existence of various instabilities as well as both first- and second-order phase transition-like behavior. For certain sets of parameters they found an amplitude self-modulation of the second harmonic and of the fundamental field in the cavity as well as new bifurcation solutions. Mandel and Erneux [105] constructed explicitly and analytically new time-periodic solutions and proved their stability in the vicinity of the transition points.

SHG equations were used also to analyze of deterministic chaos. Savage and Walls were the first [83] to prove the existence of chaos in the case of nonzero detuning between laser and cavity modes. They found a period-doubling route to chaos. Bistability, self-pulsing, and chaos were also studied Lugiato et al. [106]. The dynamics of SHG in the case of time-dependent external pumping was investigated by the present authors. Numerical analysis of the equation of motions was performed for the modulated pump amplitude [107] as well as for the external pump of rectangular pulses [108]. Alekseeva et al. [109] presented a detailed study of the spatial evolution of multifrequency fundamental and second-harmonic radiation and showed that the system may exhibit a spatial chaos due to multiple competing processes. Also, a hyperchaotic dynamic in SHG was numerically predicted [110,111].

B. Basic Equations

Let us consider an optical system with two modes at the frequencies ω and 2ω interacting through a nonlinear crystal with second-order susceptibility placed within a Fabry–Pérot interferometer. In a general case, both modes are damped and driven with external phase-locked driving fields. The input external fields have the frequencies ω_L and $2\omega_L$. The classical equations describing second-harmonic generation are [104,105]:

$$\begin{aligned} \frac{d\alpha_1}{dt} &= -i\Delta'_1\alpha_1 - \Gamma_1\alpha_1 + \kappa\alpha_1^*\alpha_2 + F_1 \\ \frac{d\alpha_2}{dt} &= -i\Delta'_2\alpha_2 - \Gamma_2\alpha_2 - \frac{1}{2}\kappa\alpha_1^2 + F_2 \end{aligned} \quad (1)$$

Rapid oscillations (at the frequencies $\omega, \omega_L, 2\omega, 2\omega_L$) are removed from Eq. (1) by frequency-matching conditions in the usual way. The quantities $\Delta'_1 = \omega - \omega_L$ and $\Delta'_2 = 2\omega - 2\omega_L$ are frequency mismatches between the cavity and external fields. Slowly varying in time, complex variables α_1 and α_2 are the electric field amplitudes of the two modes $E_1(t) = \alpha_1(t) \exp(i\omega t)$ and $E_2(t) = \alpha_2(t) \exp(2i\omega t)$

describing fundamental and second-harmonic modes, respectively. Similarly, F_1 and F_2 are proportional to the electric field amplitudes of the two external pumped modes $\mathcal{F}_1(t) = F_1(t) \exp(i\omega_L t)$ and $\mathcal{F}_2(t) = F_2(t) \exp(2i\omega_L t)$. Two constants, Γ_1 and Γ_2 , are the cavity loss rates for the appropriate modes. The coupling constant κ between the two modes is proportional to a nonlinear susceptibility $\chi^{(2)}$ of the nonlinear medium. With a special choice of the spatial mode functions, we can assume that κ is real, and we exclude from our investigation of polarization effects — all fields have linear polarization in the same directions [104].

For numerical investigation, it is convenient to reduce the number of relevant parameters in Eq. (1). On substituting

$$\tau = \kappa t, \quad \Delta_{1(2)} = \frac{\Delta'_{1(2)}}{\kappa}, \quad \gamma_{1(2)} = \frac{\Gamma_{1(2)}}{\kappa}, \quad f_{1(2)}(\tau) = \frac{F_{1(2)}(\tau/\kappa)}{\kappa} \quad (2)$$

into (2), we get the following redefined set of equations:

$$\begin{aligned} \frac{d\alpha_1}{d\tau} &= -i\Delta_1\alpha_1 - \gamma_1\alpha_1 + \alpha_1^*\alpha_2 + f_1(\tau) \\ \frac{d\alpha_2}{d\tau} &= -i\Delta_2\alpha_2 - \gamma_2\alpha_2 - \frac{1}{2}\alpha_1^2 + f_2(\tau) \end{aligned} \quad (3)$$

where f_i are taken to be real. The above equations can be written in real variables. On inserting

$$\begin{aligned} \alpha_1 &= \text{Re}(\alpha_1) + i \text{Im}(\alpha_1) = y_1 + i y_3 \\ \alpha_2 &= \text{Re}(\alpha_2) + i \text{Im}(\alpha_2) = y_2 + i y_4 \end{aligned} \quad (4)$$

we obtain four equations of motion:

$$\begin{aligned} \frac{dy_1}{dt} &= \Delta_1 y_3 - \gamma_1 y_1 + y_1 y_2 + y_3 y_4 + f_1 \\ \frac{dy_2}{dt} &= \Delta_2 y_4 - \gamma_2 y_2 - \frac{1}{2}(y_1^2 - y_3^2) + f_2 \\ \frac{dy_3}{dt} &= -\Delta_1 y_1 - \gamma_1 y_3 + y_1 y_4 - y_2 y_3 \\ \frac{dy_4}{dt} &= -\Delta_2 y_2 - \gamma_2 y_4 - y_1 y_3 \end{aligned} \quad (5)$$

These four equations of motion describe the dynamics of SHG in the four-dimensional phase space $(\text{Re} \alpha_1, \text{Im} \alpha_1, \text{Re} \alpha_2, \text{Im} \alpha_2)$. In practice, we can observe the motion only in the reduced phase space (phase surface). For example, with

the help of two-dimensional phase portraits $(\text{Re}\alpha_i, \text{Im}\alpha_j)$, $(\text{Re}\alpha_i, \text{Re}\alpha_j)$ and $(\text{Im}\alpha_i, \text{Im}\alpha_j)$, we can qualify the kind of motion of our system, which may be periodic, quasiperiodic, or chaotic.

To identify chaotic behavior of a dynamical system, it is convenient to use the *Lyapunov exponents* [112,113]. In particular, the procedure proposed by Wolf et al. [114] is a very useful and efficient method that gives such exponents. In this method we have to linearize the set of equations (5), and next the linearized equations are solved together with the primary equations. Moreover, we solve the eigenproblem for the Jacobi matrix of the set of linearized equations in the so-called tangent space. Then, after Gram–Schmidt reorthonormalization, we obtain the set of Lyapunov exponents λ_i as eigenvalues of the long-time product Jacobi matrix. So, in this method the number of exponents, is equal to a dimension of phase space [115]. In our case we have a set $\{\lambda_1\lambda_2\lambda_3\lambda_4\}$; thus, we get a *spectrum* of Lyapunov exponents. Such a spectrum is ordered from maximal to minimal value. The quantity λ_1 is traditionally termed the *maximal Lyapunov exponent* (MLE), and its positive value points to chaotic motion. If $\lambda_1 \leq 0$, the dynamical system behaves nonchaotically (orderly).

A highly unstable system can manifest hyperchaotic behavior [116]. This means that we have two positive Lyapunov exponents in a spectrum. The phenomenon of hyperchaos have been investigated in many papers [117–120]. A route to hyperchaos was also investigated [121], and a method of controlling of hyperchaos was introduced [122].

In next three sections we present a short overview of investigations of chaotic and hyperchaotic behavior in the process of SHG.

C. Simplest Case: $\gamma_i = 0$, $\Delta_i = 0$, $f_i = 0$

In the simplest case of a free evolution without damping, pumping, and mismatch, the equations of motion (3) are solved analytically. One easily notes that the system (3) now belongs to the class of Hamiltonian systems with two constants of motion:

$$\begin{aligned} I_1 &= \alpha_1^* \alpha_1 + 2\alpha_2^* \alpha_2 \\ I_2 &= -\frac{1}{2}i (\alpha_1^2 \alpha_2^* - \alpha_2 \alpha_1^{*2}) \end{aligned} \quad (6)$$

They reduce the set (5) of four equations in real variables to two equations. This means that we can have only regular, periodic, or quasiperiodic behavior, never chaos. Chaos in a dynamical system governed by ordinary differential equations can arise only if the number of equations is equal to or greater than 3. We remember that we refer to the case of perfect phase matching ($\Delta k = k_1 - 2k_2 = 0$), and the well-known monotonic evolution of fundamental and

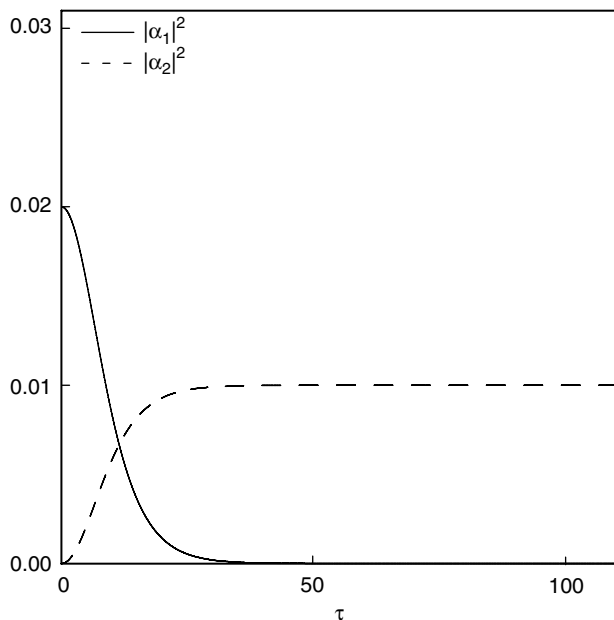


Figure 1. Monotonic behaviour of the fundamental and second-harmonic modes. Solution of Eqs. (7) for the initial conditions $\alpha_{10} = 0.1 + i0.1$ and $\alpha_{20} = 0$.

second-harmonic mode intensities has been found [99,102] and is shown on Fig. 1. If $\Delta k \neq 0$, we obtain three equations of motion for α_1 , α_2 , Δk (six equations in real variables) and well known solutions show an oscillation behavior in such cases of SHG. Detailed analyses are available in the literature [99,102,103].

Let us focus on the role of initial conditions in this case of SHG. The equations of motion

$$\frac{d\alpha_1}{d\tau} = \alpha_1^* \alpha_2, \quad \frac{d\alpha_2}{d\tau} = -\frac{1}{2} \alpha_1^2 \quad (7)$$

were solved with initial conditions $\alpha_1(0) = \alpha_{10}$ and $\alpha_2(0) = \alpha_{20}$. The case of $(\alpha_{10} \neq 0, \alpha_{20} = 0)$ is often called a *second-harmonic generation process* (Fig. 1). For the case of $(\alpha_{10} \neq 0, \alpha_{20} \neq 0)$, that is, when both fields start from the nonzero initial conditions, we deal with a mixed process of sub/second-harmonic generation. Throughout this work the symbol SHG refers to both these cases. In Fig. 2 we see the evolution of the system from the initial conditions: $\alpha_{10} = 0.1 + i0.1$ and $\alpha_{20} = 0.01 + i0.01$. One can observe in Fig. 2a the periodic oscillation in intensity of both modes. However, in the phase space the motion of

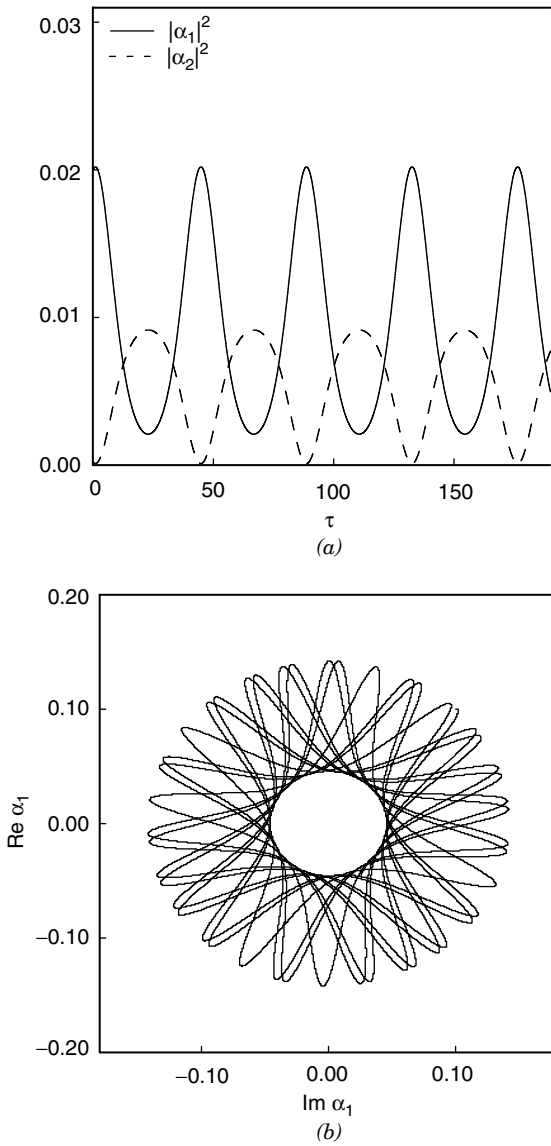


Figure 2. Time evolution of intensity (a) and phase portrait for the fundamental mode (b). Solution of Eqs. (7) for the initial conditions $\alpha_{10} = 0.1 + i0.1$ and $\alpha_{20} = 0.01 + i0.01$. Quasi-periodic behavior.

the system is quasiperiodic, as seen in Fig. 2b. The phase point draws a nonclosed path within the rosette area. The rosette becomes increasingly denser with time, and finally we get a blackened area. A similar rosette is obtained for the second-harmonic mode. For the case of $(\alpha_{10} = 0, \alpha_{20} \neq 0)$, Eq. (7) have constant solutions, and we do not observe any time changes in the SHG system. There is no subharmonic generation without an external pumping f_2 .

To sum up, in nonlinear systems the influence of initial conditions on dynamics of a system is essential, therefore the three different initial conditions discribed above lead to different dynamics within the same equations of motion.

D. Coherent External Field

Another clear example of a system generating second harmonics is the one employing an external coherent pump field $f_i = \text{constant}$ without dumping ($\gamma_i = 0$) and frequency mismatch ($\Delta_i = 0$). The system belongs to the class of Hamiltonian systems. The function (Hamiltonian)

$$H(\tau) = if_1 (\alpha_1^* - \alpha_1) + if_2 (\alpha_2^* - \alpha_2) - \frac{1}{2}i(\alpha_1^2\alpha_2^* - \alpha_2\alpha_1^{*2}) \quad (8)$$

is a constant of motion for Eq. (3). Since we have only pumping, the trajectory shows an expanding nature [123].

If we now include damping (without mismatch), we get results in compliance with Ref. 104. As did Mandel and Erneux [105], we introduce the notions of good ($\gamma_1 \ll \gamma_2$) and bad ($\gamma_1 \cong \gamma_2$) frequency conversion limits in our discussions. We denote them as GCL and BCL, respectively. The case of a coherent pump field was also studied by Drummond et al. [104] with a nonrescaled version of Eq. (1). To get the compact results we use, in accordance with (3), the parameters $f_0 = 2$, $\tau = 10t$, and $\gamma_1 = \gamma_2 = 0.34$ (BCL) or $\gamma_1 = 0$, $\gamma_2 = 0.34$ (GCL). For the intensity of the coherent pump

$$f_1 = (2\gamma_1 + \gamma_2)\sqrt{2\gamma_2(\gamma_1 + \gamma_2)} \quad (9)$$

and $f_2 = 0$, we get a transition from monotonic solutions of (3) to a self-pulsation. As we see in Fig. 3a, after transient effects the system manifests self-pulsation and an appropriate phase portrait for the fundamental mode is presented in Fig. 3b. The limit cycle indicates a periodic motion of the system. If the pump f_1 increases some multiperiodic oscillations occur (Fig. 4). If we change the parameters of pumping f_1 and f_2 , we can find [104] that this system exhibits both first- and second-order phase transition-like behavior and also has a hard mode transition. Farther numerical and analytical analysis [105] indicated a new transition involves an hysteresis cycle.

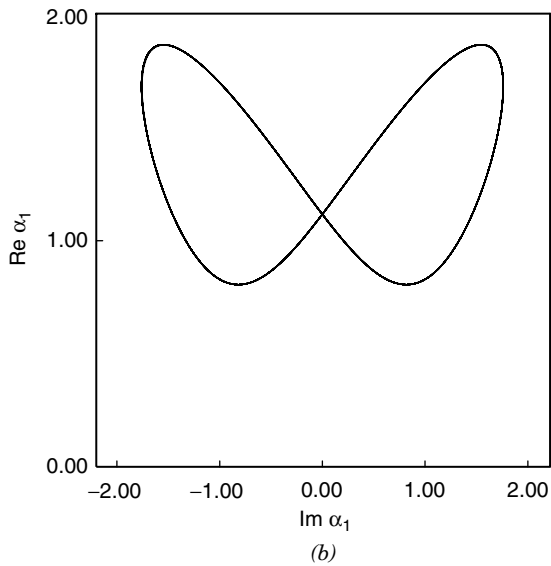
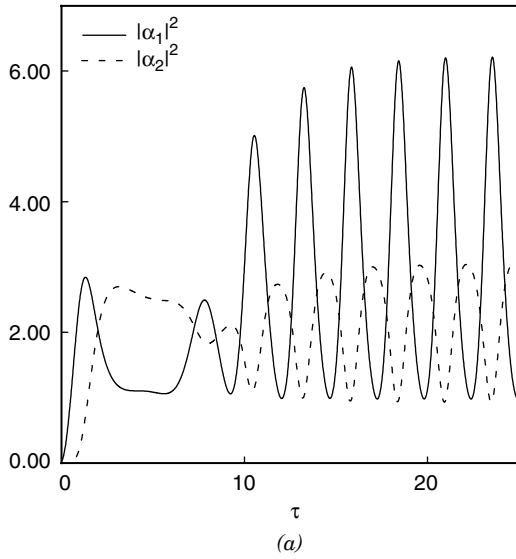


Figure 3. Time evolution of intensity (a) and phase portrait for the fundamental mode (b). Solution of Eqs. (3) for $f_1 = 2$, $f_2 = 0$, $\gamma_1 = \gamma_2 = 0.34$ (BCL) and initial conditions $\alpha_{10} = 0.1 + i 0.1$ and $\alpha_{20} = 0$. Self-pulsation.

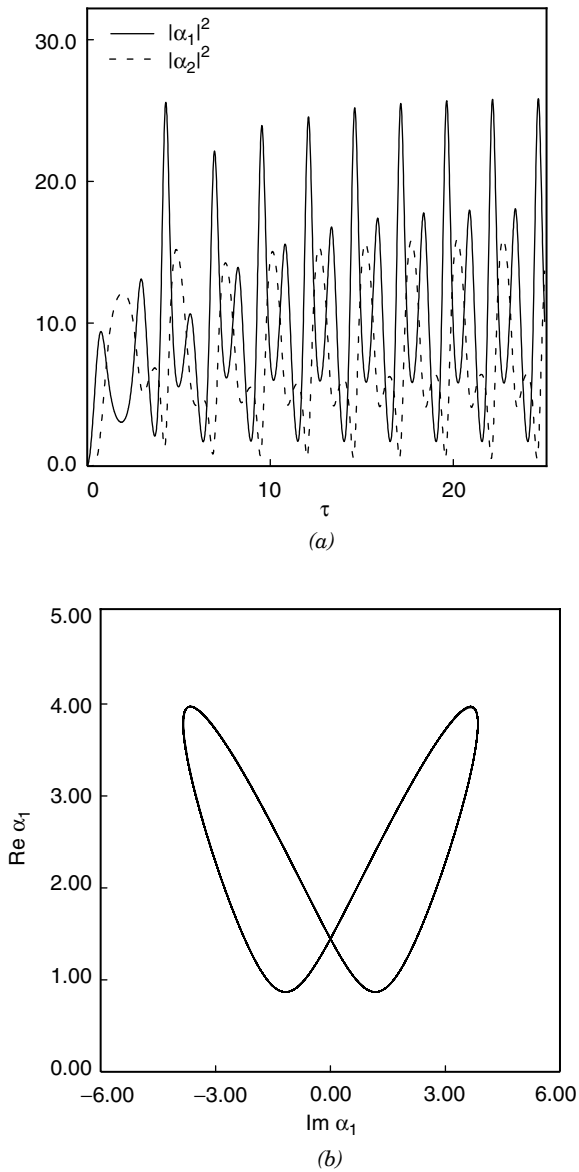


Figure 4. Multiperiodic behaviour in SHG. The same as in Fig. 3 but $f_1 = 5$.

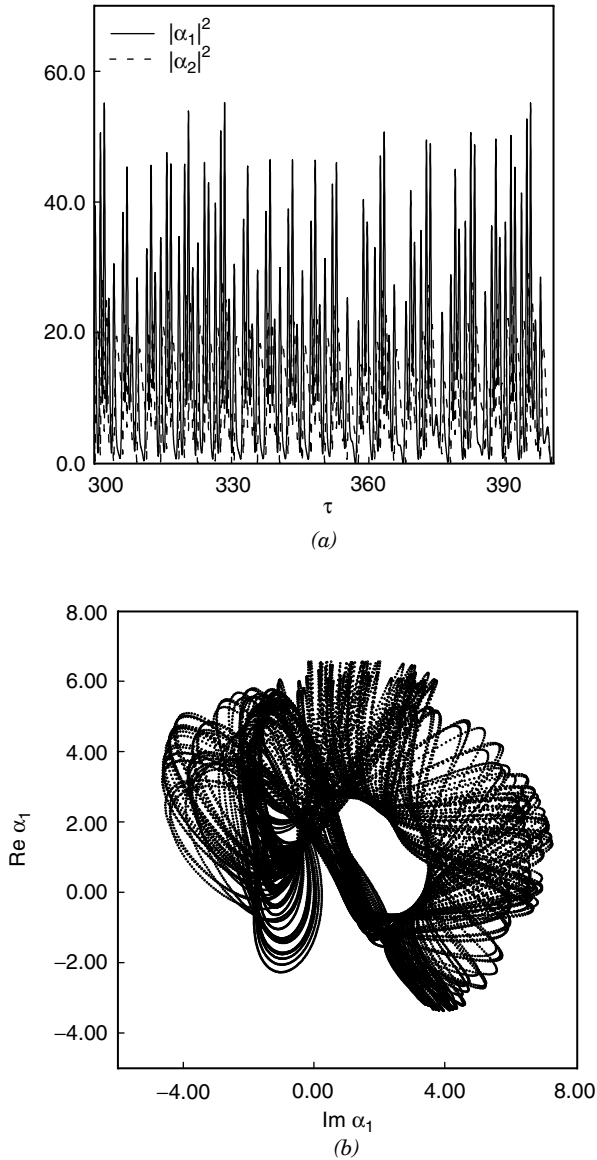


Figure 5. Time evolution of intensity (a) and phase portrait for the fundamental mode (b). Solutions of Eqs. (3) with parameters $\Delta_1 = \Delta_2 = 1, f_1 = 5.5, f_2 = 0, \gamma_1 = \gamma_2 = 0.34$ (BCL). The initial conditions are $\alpha_{10} = 0.1 + i0.1$ and $\alpha_{20} = 0.01 + i0.01$. Chaos.

We get a very similar time behavior in subharmonic generation where $f_1 = 0$ and $f_2 \neq 0$. Self-pulsation and multiperiodic evolution of intensities have been found. However, these findings are not investigated here.

The case of a frequency mismatch between laser pumps and cavity modes was investigated [83], and for the first time, chaos in SHG was found. When the pump intensity is increased, we observe a period doubling route to chaos for $\Delta_1 = \Delta_2 = 1$. Now, for $f_1 = 5.5$, Eq. (3) give aperiodic solutions and we have a chaotic evolution in intensities (Fig. 5a) and a chaotic attractor in phase plane ($\text{Im } \alpha_1, \text{Re } \alpha_1$) (Fig. 5b).

E. Modulated External Field

A more complicated behavior of the system (3) is manifested if the time-dependent driving field and damping are taken into account. Let us assume that the driving amplitude has the form $f_1(\tau) = f_0(1 + \sin(\Omega\tau))$, meaning that the external pump amplitude is modulated with the frequency Ω around f_0 . Moreover, $f_2 = 0$ and $\Delta_1 = \Delta_2 = 0$. It is obvious that if we now examine Eq. (3), the situation in the phase space changes sharply. In our system there are two competitive oscillations. The first belongs to the multiperiodic evolution mentioned in Section II.D, and the second is generated by the modulated external pump field. Consequently, we observe a rich variety of nonlinear oscillations in the SHG process.

The frequency of modulation Ω is now the main parameter, and we are able to switch the system of SHG between different dynamics by changing the value of Ω . To find the regions of Ω where a chaotic motion occurs, we calculate a Lyapunov spectrum versus the “knob” parameter Ω . The first Lyapunov exponent λ_1 from the spectrum is of the greatest importance; its sign determines the chaos occurrence. The maximal Lyapunov exponent λ_1 as a function of Ω is presented for GCL in Fig. 6a and for BCL in Fig. 6b. We see that for some frequencies Ω the system behaves chaotically ($\lambda_1 > 0$) but orderly ($\lambda_1 < 0$) for others. The system in the second case is much more damped than in the first case and consequently much more stable. By way of example, for $\Omega = 0.9$ the system of SHG becomes chaotic as illustrated in Fig. 7a, showing the evolution of second-harmonic and fundamental mode intensities. The phase point of the fundamental mode draws a chaotic attractor as seen in the phase portrait (Fig. 7b). However, the phase point loses its chaotic features and settles into a symmetric limit cycle if we change the frequency to $\Omega = 1.1$ as shown in Fig. 8b, while Fig. 8a shows a seven-period oscillation in intensities. To avoid transient effects, the evolution is plotted for $450 < \tau < 500$.

Let us emphasize that for other values of parameter Ω we can also observe in the phase plane intricate symmetric limit cycles [107,123], such as the five-period oscillations we get for $\Omega = 0.78$.

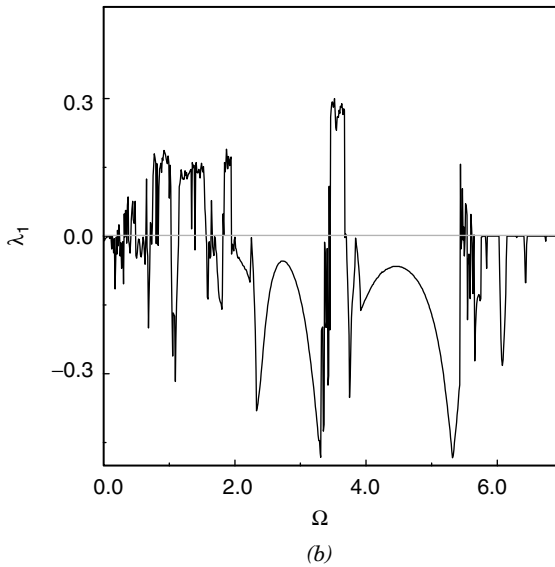
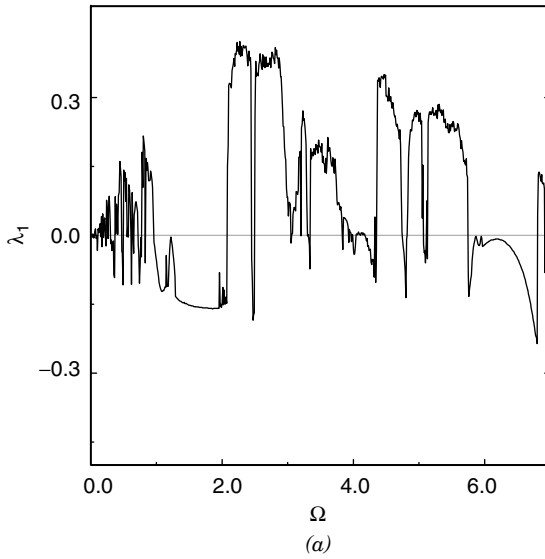


Figure 6. Maximal Lyapunov exponent λ_1 versus the modulation parameter Ω for $f_0 = 2$ and the initial conditions are $\alpha_{10} = 0.1 + i0.1$ and $\alpha_{20} = 0.01 + i0.01$. (a) GCL and (b) BCL.

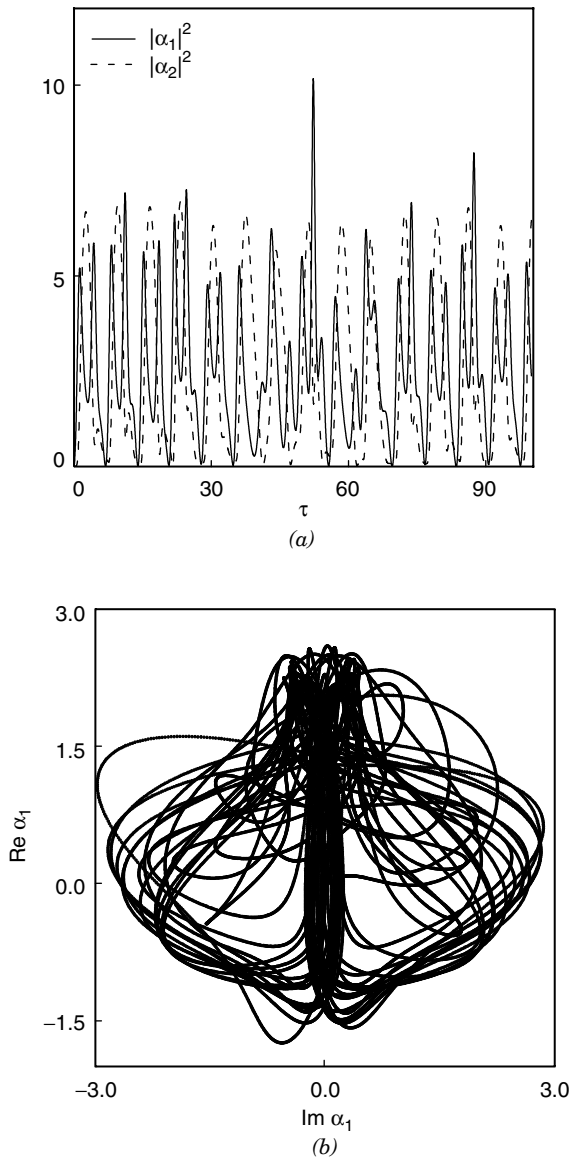


Figure 7. Time evolution of intensity (a) and phase portrait for the fundamental mode for $0 < \tau < 300$ (b). Parameters are the same as in Fig. 6b (BCL), but with $\Omega = 0.9$. Chaos.

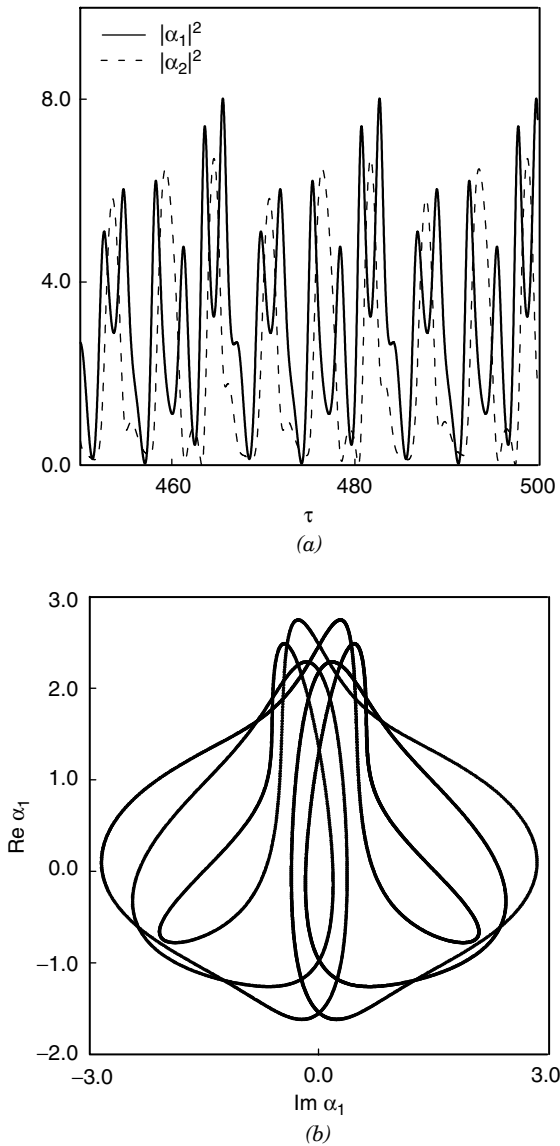


Figure 8. Time evolution of intensity (a) and phase portrait for the fundamental mode for $\tau > 450$ (b). Parameters are the same as in Fig. 6b (BCL) but with $\Omega = 1.1$. Limit cycle.

Highly unstable systems lead to two positive Lyapunov exponents that show the *hyperchaotic* behavior [116]. Now, Eq. (3) is numerically examined with damping constants $\gamma_1 = \gamma_2 = 0.01$. In Fig. 9a we see only the two largest Lyapunov exponents of all the spectrum *versus* the modulation parameter Ω . The

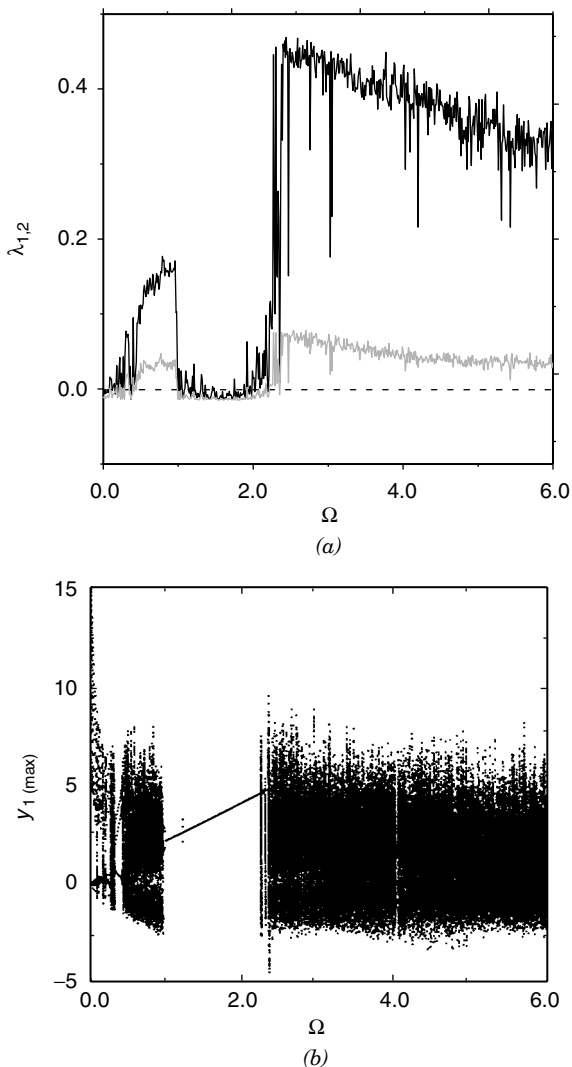


Figure 9. The two largest Lyapunov exponents (a) and the bifurcation diagram (the maxima of y_1) (b) versus the modulation parameter Ω . Parameters are $f_0 = 1$, $\gamma_1 = \gamma_2 = 0.01$ and the initial conditions are $\alpha_{10} = 0.1 + i0.1$ and $\alpha_{20} = 0.01 + i0.01$. Hyperchaos.

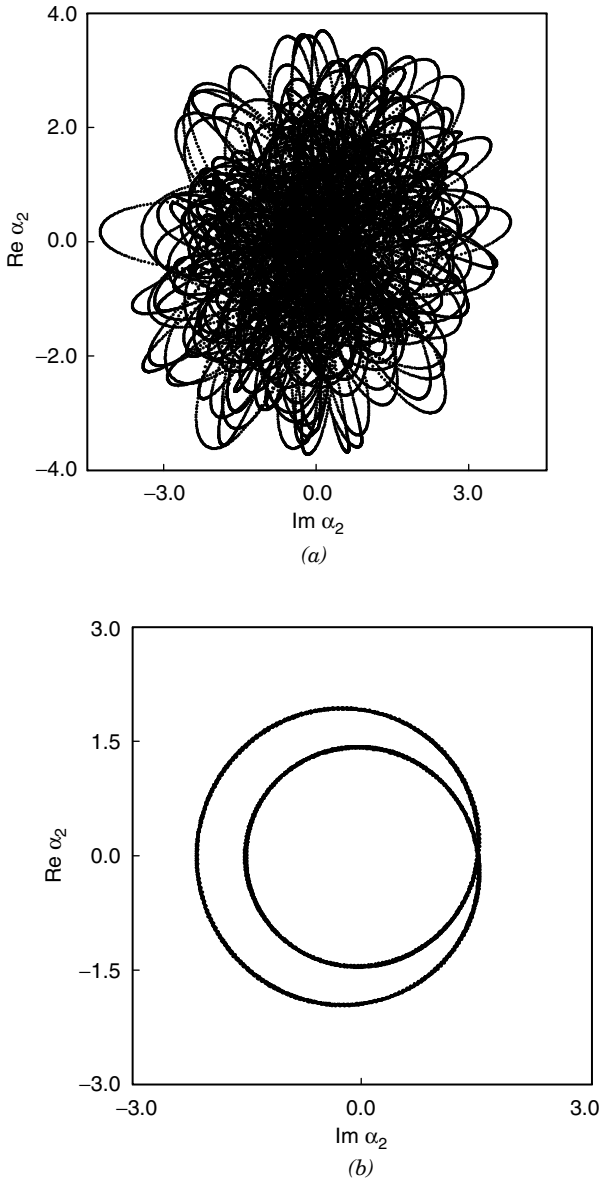


Figure 10. The phase portraits $\text{Re } \alpha_2$ versus $\text{Im } \alpha_2$ for $f_0 = 1$, $\gamma_1 = \gamma_2 = 0.01$, $\alpha_{10} = 0.1 + i0.1$, and $\alpha_{20} = 0.01 + i0.01$. The hyperchaotic trajectory for $\Omega = 0.8$ (a) and the limit cycle for $\Omega = 1.55$ (b). The time is $400 < \tau < 500$.

damping is so weak that we can state that the system is hyperchaotic. There are two extensive regions of hyperchaos between $0.45 < \Omega < 0.98$ and $\Omega > 2.22$, where two Lyapunov exponents are positive. In the region $0.98 < \Omega < 2.22$ hyperchaos does not appear at all. Generally, the region $0.98 < \Omega < 2.22$ can be treated as nonchaotic apart from a few values of the parameter Ω for which only one Lyapunov exponent is positive. These regions of stability and instability are best visualized in the bifurcation diagram (Fig. 9b), where we plot the maxima of $\text{Re } \alpha_1 = y_1$ versus the parameter of modulation Ω . It is obvious that a change in Ω switches the system among chaos, hyperchaos, or limit cycles. For $\Omega = 0.8$, we observe a hyperchaotic orbit in the phase portrait of the second-harmonic mode (Fig. 10a). The same orbit, except for $\Omega = 1.55$, becomes a limit cycle (Fig. 10b).

When the damping in the system is increased, the regions of hyperchaos disappear. Moreover, it is interesting that the region of order that we obtained in Fig. 9 is very stable despite changing damping constants, so we can choose the frequency of modulation of an external field in such a way ($1 < \Omega < 1.8$) that the system remains stable even for a relatively small damping.

F. Pulsed External Field

In this section we consider a case particularly important for experimental investigation. The external driving field $f_1(\tau)$ applied to Eq. (3) has the form of a train of pulses that are simulated by a computer. The length of the pulse is denoted by T_1 , and the height of the pulse by f_0 . The distance between two pulses is denoted by T_2 . For $f_0 \neq 0$ and $T_2 = 0$, the train of pulses becomes a coherent driving field (Section II.D). The second driving field f_2 is assumed to be zero and $\Delta_1 = \Delta_2 = 0$. We examine the dynamical system (3) in the same way as in Section II.E. In Fig. 11 we present the maximal Lyapunov exponent λ_1 as a function of the length of the pulse T_1 (for $T_2 = 1$). As shown in Fig. 11a,b, at the beginning λ_1 is negative, implying the appearance of order in the range $0 < T_1 < 0.085$ for GCL and $0 < T_1 < 0.55$ for BCL. The fundamental ($|\alpha_1|^2$) and second-harmonic ($|\alpha_2|^2$) intensities tend to oscillatory states in the course of time [108]. This is the short-pulse regime, and the appropriate evolution of both intensities is shown in Fig. 12. Here, one can easily recognize moments of time where the pulses are switched on and off. The period of sawtooth-like oscillations is equal to the repetition rate of pulses. The typical phase portrait for the short-pulse case is presented in Fig. 13. Finally, we observe a limit cycle where the phase point moves up and down only a segment of a straight line (shaded dark in Fig. 13b).

For $0.085 < T_1 < 0.5$ (GCL) and for $0.55 < T_1 < 0.97$ (BCL), the maximal Lyapunov exponents λ_1 are near zero; consequently, we obtained quasiperiodic trajectories. Typical quasiperiodic trajectories for both cases are shown in

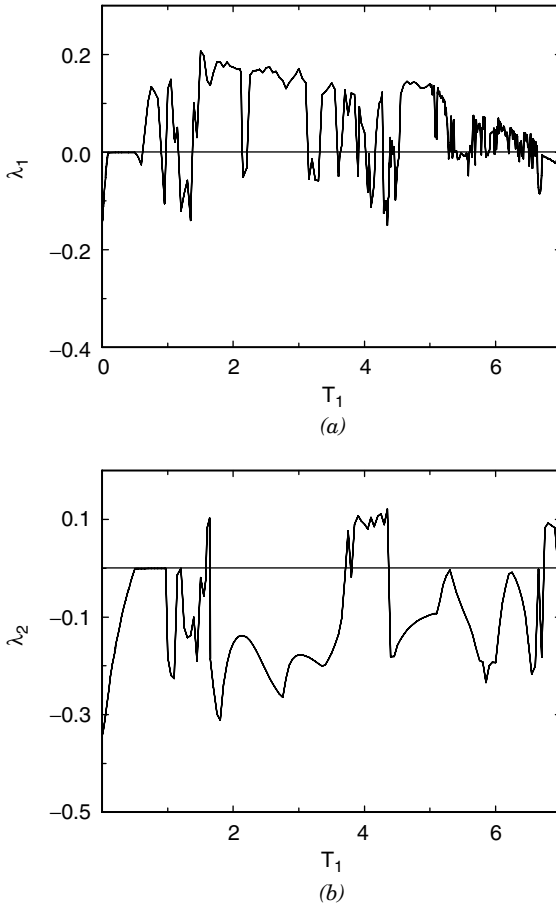


Figure 11. The maximal Lyapunov exponent λ_1 versus the pulse duration T_1 , for $f_0 = 2, T_2 = 1, \alpha_{10} = 0.1 + i0.1, \alpha_{20} = 0$: (a) the case of GCL $\gamma_1 = 0, \gamma_2 = 0.34$; (b) the case of BCL $\gamma_1 = 0.34, \gamma_2 = 0.34$.

Fig. 14. The trajectory is a nonclosed path, and for long times we get a blackened area.

A more complicated behavior of the MLE is observed for higher values of T_1 . Varying the length of the pulse T_1 , we observe regions of order and chaos. By way of an example, the phase portrait $\text{Re}\alpha_1$ versus $\text{Im}\alpha_1$ for a chaotic attractor is shown in Fig. 15.

Within the region of order ($\lambda_1 \leq 0$) we see intricate symmetric and non-symmetric limit cycles in phase diagrams. For example, for $T_1 = 4.1$ we see in

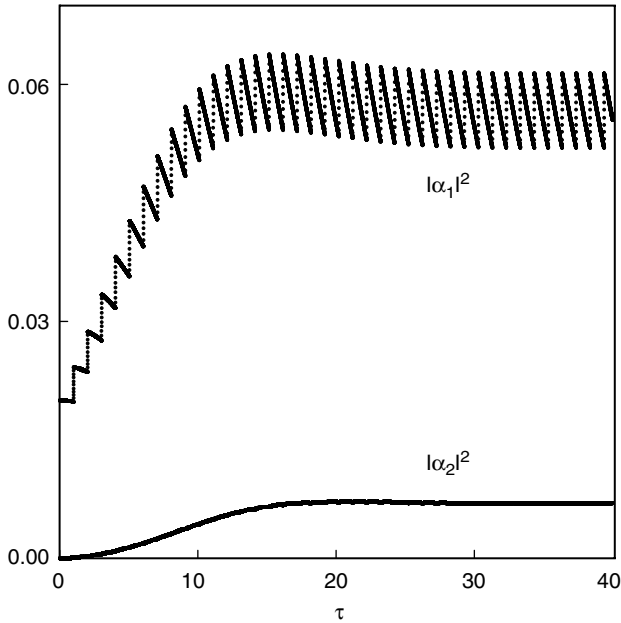


Figure 12. Intensities in the short-pulse regime for the GCL case. The parameters are the same as for Fig. 11a but $T_1 = 0.01$.

Fig. 16a symmetric limit cycles for the second-harmonic mode (GCL) and in Fig. 16b, an nonsymmetric phase portrait example for $T_1 = 0.5$ for BCL. In both cases the phase point settles down into a closed-loop trajectory, although not earlier than about $\tau > 200$. An intricate limit cycle is usually related to multiperiod oscillations. For example, the cycle in Fig. 16a corresponds to five-period oscillations of the fundamental and SHG modes intensity, and the phase portrait in Fig. 16b resembles the four-period oscillations (see Fig. 17). Generally, for $T_1 > 0.5$, we observe many different multiperiod (even 12-period) oscillations in intensity and a rich variety of phase portraits.

Some hyperchaotic behavior in SHG with pump of pulses has been shown [111]. The two largest Lyapunov exponents versus a duration of pulse T_1 are presented in Fig. 18a for the cases of BCL. There are a two regions of hyperchaos. A Typical hyperchaotic phase portrait is presented in Fig. 18b.

G. Final Remarks

Small changes in the modulated pump parameters Ω, f_o and in the pulse parameters T_1, T_2, f_o induce dramatic changes the output fields. Therefore

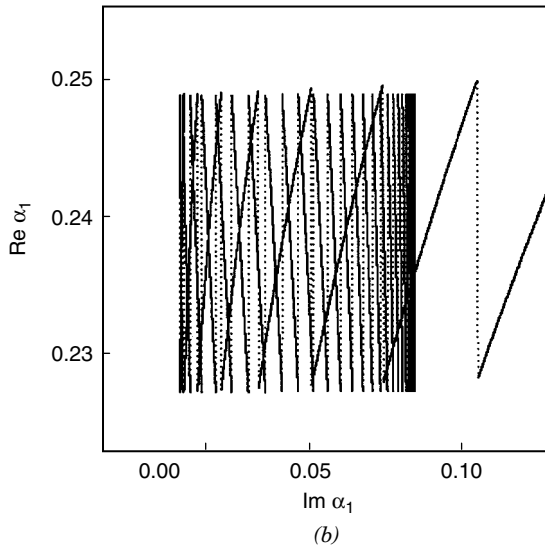
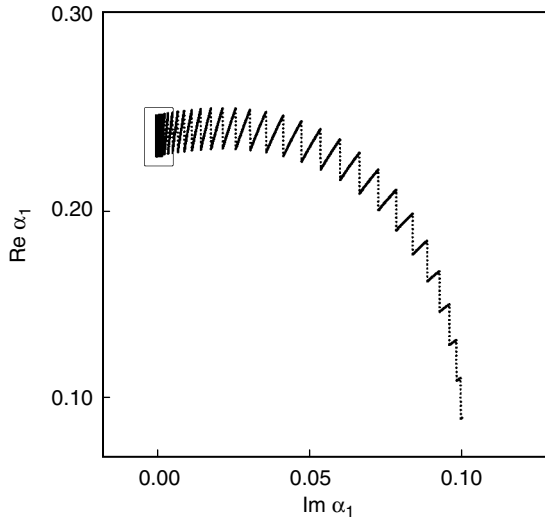


Figure 13. (a) A typical phase portrait in the short-pulse regime for GCL case; (b) an enlargement of the signed region of Fig. 13a. The parameters are the same as for Fig. 11a but $T_1 = 0.01$.

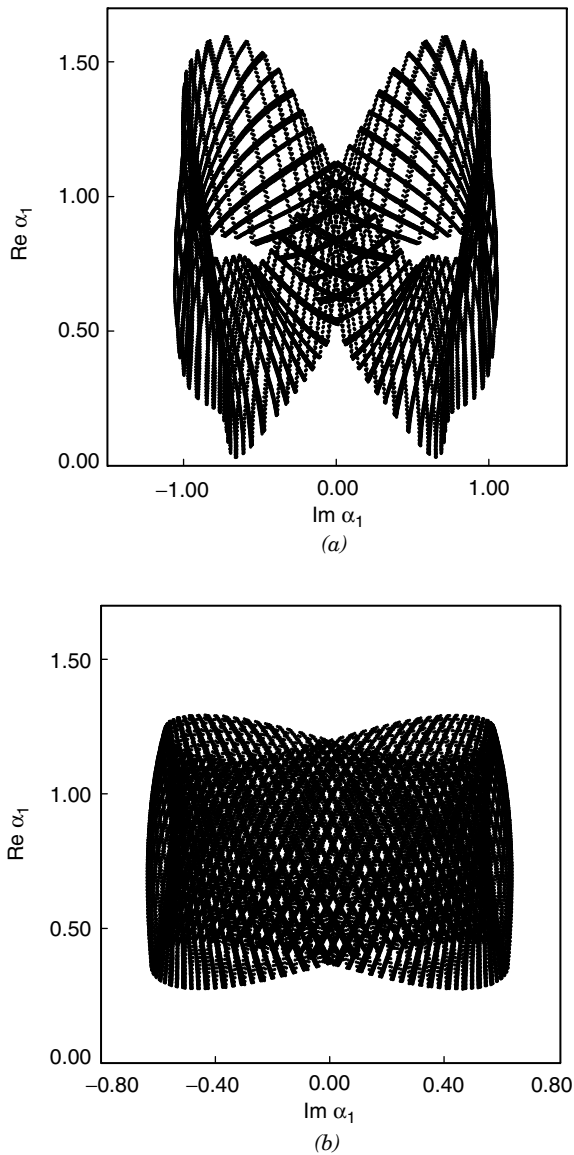


Figure 14. Quasiperiodic orbits for the parameters of Fig. 11 but (a) $T_1 = 0.5$ (GCL) and (b) $T_1 = 0.8$ (BCL). The time is $0 \leq \tau \leq 300$.

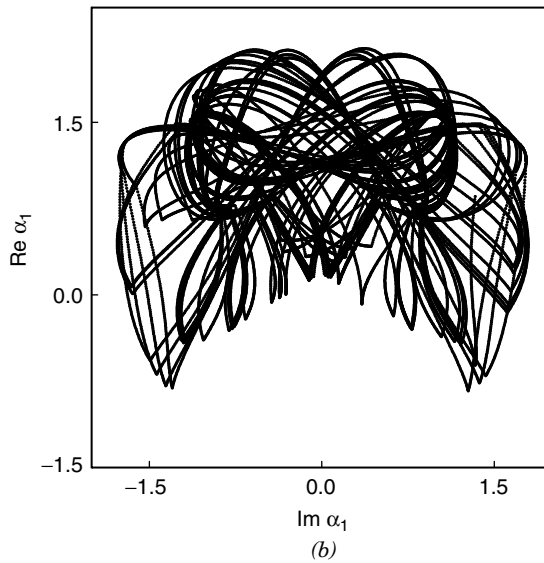
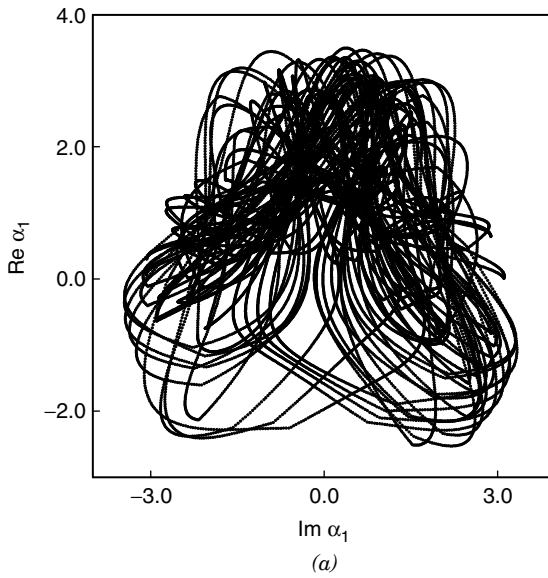


Figure 15. Chaotic attractors for the parameters of Fig. 11 but $T_1 = 0.5$ (GCL) (a) and $T_1 = 4$ (BCL) (b). The time is $0 \leq \tau \leq 300$.

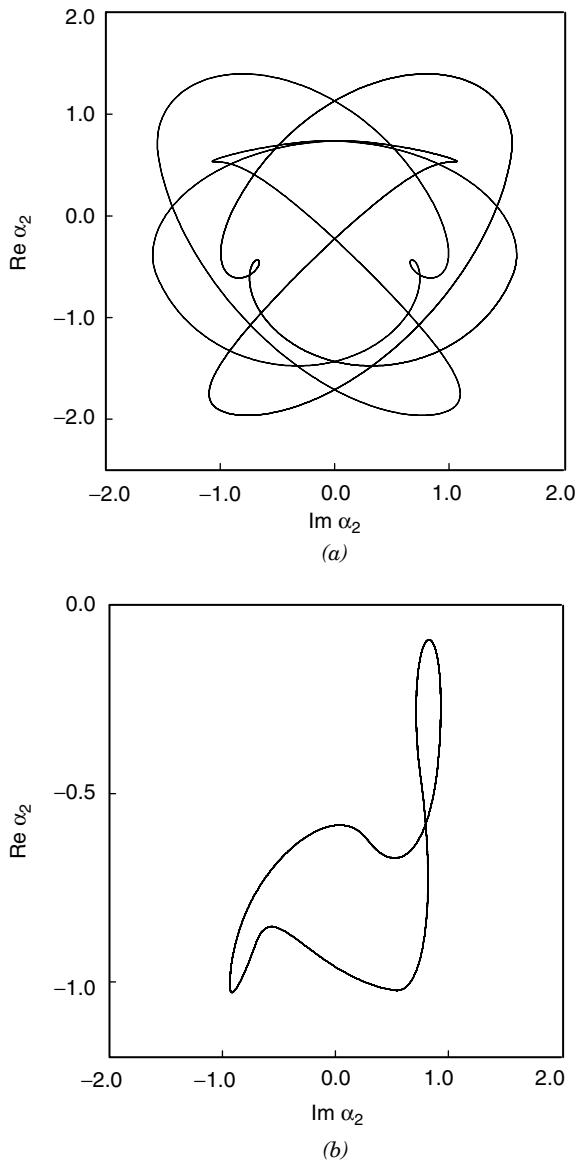


Figure 16. Phase portraits for the second-harmonic mode: (a) symmetric example for GCL, (b) nonsymmetric example for BCL. The parameters are the same as for Fig. 11, and the time is $200 < \tau < 500$.

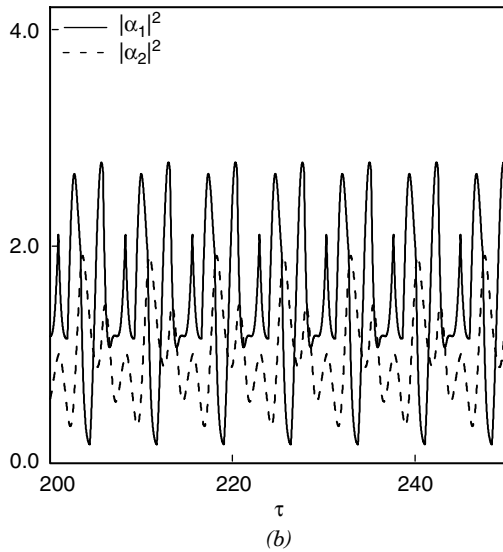
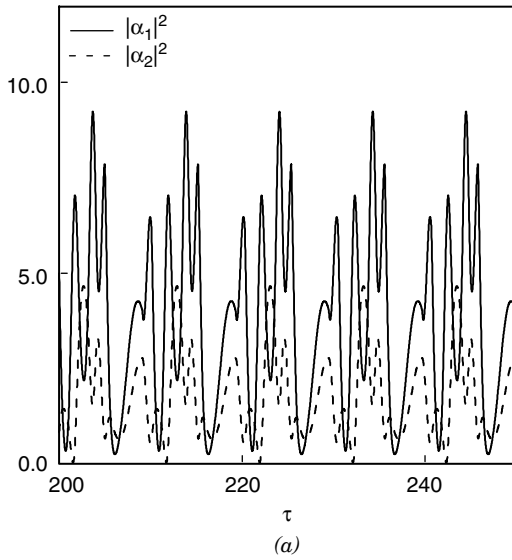


Figure 17. Evolution of the intensities related to the cases of Fig. 16: (a) five-period oscillations in GCL; (b) four-period oscillations in BCL.

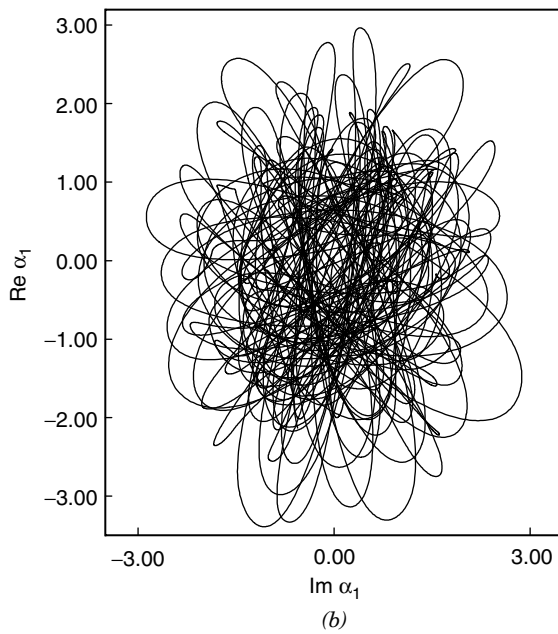
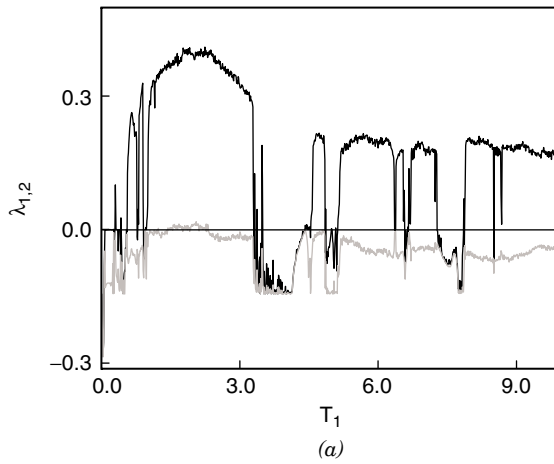


Figure 18. (a) The two largest Lyapunov exponents λ_1 and λ_2 versus the pulse duration T_1 , for $f_0 = 2$, $\alpha_{10} = 0.1 + i0.1$, $\alpha_{20} = 0$ and for BCL; (b) typical hyperchaotic phase portrait for pulse duration $T_1 = 2.0$.

SHG can be used as a source of signals with chaotic or even hyperchaotic amplitudes that can be suddenly switched to the periodic regimes. This kind of performance can be employed for communications devices. We mention here the possibility of encoding a message within chaotic dynamics [124].

In order to relate the theory and numerical calculations to the physical parameters, we followed the estimations of Drummond et al. [104]. For a typical spherical Fabry–Pérot interferometer of length 10 cm with an appropriate crystal (e.g., KDP of length 1 cm), one can get approximate values of parameters of the SHG system. The typical damping constant for the mirror reflectivities 0.995 is $\gamma \simeq 10^6$. The coupling constant κ was estimated in the interval of 50–500 s^{-1} . These coupling constant values permit experimental verification of dynamical behavior of SHG. In preceding, sections the coupling constant κ is given by relation $\kappa = \tau/t$, where τ and t are the rescaled and real times, respectively. Therefore the parameter of modulation Ω can change between 0 and 3500 Hz (in our calculations $0 < \Omega < 7$ in arbitrary units). We also obtained the appropriate pulse repetition rate in an interval from 10^{-3} up to 10^{-2} s. This rather rough estimation allows experimental verification of our numerical analysis.

III. CHAOS IN KERR OSCILLATORS

A. Introduction

Since 1990 considerable interest has been devoted to mutually coupled dynamical systems. Different kinds of new dynamical behavior have been revealed and studied, including synchronization effects [125–128], ON-OFF intermittency [129], two-state ON-OFF intermittency [130], uncertain destination dynamics [131], or riddled basins of attractions [132]. Other interesting topics in the field of coupled nonlinear systems are generation of beats and their properties. The structure of beats has been intensely studied mainly in quantum and nonlinear optics. The intricate beats are frequently referred to as “revivals” and “collapse phenomena” [133]. The revivals and collapses, representing the structure of complicated modulations, remain quasiperiodic functions [134,135]. It is well known that beats in linear systems originate from the superposition of periodic functions with slightly different periods. The question is what are the changes in the structure of beats in a linear system if the linear system is supplemented by a nonlinear term and whether it is possible to generate chaotic beats.

One of the best known and most intensively studied optical models is an oscillator with Kerr nonlinearity. Mutually coupled Kerr oscillators can be successfully used for a study of couplers; the systems consist of a pair of coupled Kerr fibers. The first two-mode Kerr coupler was proposed by Jensen [136] and investigated in depth [136,137]. Kerr couplers affected by quantization can

exhibit various quantum properties such as squeezing of vacuum fluctuations, sub-Poissonian statistics, collapses, and revivals [138,139].

In this section we consider a model of interactions between the Kerr oscillators applied by J. Fiurášek et al. [139] and Peřinová and Karská [140]. Each Kerr oscillator is externally pumped and damped. If the Kerr nonlinearity is turned off, the system is linear. This enables us to perform a simple comparison of the linear and nonlinear dynamics of the system, and we have found a specific nonlinear version of linear filtering. We study numerically the possibility of synchronization of chaotic signals generated by the Kerr oscillators by employing different feedback methods.

B. Basic Equations

The Hamilton function for a single Kerr oscillator is defined by

$$H(p, q) = \frac{p^2}{2} + \frac{\omega_0^2 q^2}{2} + \epsilon \left(\frac{p^2}{2} + \frac{\omega_0^2 q^2}{2} \right)^2 \quad (10)$$

where ϵ is the Kerr parameter. If $\epsilon = 0$, the Hamiltonian expressed here describes a simple harmonic oscillator with the natural frequency ω_0 . The dynamical variables p and q denote the momentum and generalized coordinate, respectively. The Hamilton equations

$$\frac{dq}{dt} = \frac{\partial H}{\partial p} \quad (11)$$

$$\frac{dp}{dt} = -\frac{\partial H}{\partial q} \quad (12)$$

applied to the Hamiltonian (10) lead to the following coupled equations of motion:

$$\frac{dq}{dt} = p[1 + \epsilon(p^2 + \omega_0^2 q^2)] \quad (13)$$

$$\frac{dp}{dt} = -\omega_0^2 q[1 + \epsilon(p^2 + \omega_0^2 q^2)] \quad (14)$$

If the initial state of the system is determined by the initial conditions $q(0) = q_0$ and $p(0) = p_0$, the solution of the system (13)–(14) is given by

$$q(t) = q_0 \cos \omega_0 [1 + \epsilon(p_0^2 + \omega_0^2 q_0^2)]t + \frac{p_0}{\omega_0} \sin \omega_0 [1 + \epsilon(p_0^2 + \omega_0^2 q_0^2)]t \quad (15)$$

$$p(t) = p_0 \cos \omega_0 [1 + \epsilon(p_0^2 + \omega_0^2 q_0^2)]t - q_0 \omega_0 \sin \omega_0 [1 + \epsilon(p_0^2 + \omega_0^2 q_0^2)]t \quad (16)$$

The system (13)–(14) has two independent constants of motion (first integrals): the Hamilton function (10) and

$$\phi(p, q; t) = -\omega_0 [1 + \epsilon(p^2 + \omega_0^2 q^2)]t + \arctan\left(\frac{\omega_0 q}{p}\right) \quad (17)$$

For $\epsilon = 0$, the quantities (10) and (17) become first integrals for the harmonic oscillator [141]. It is obvious from (15)–(16) that a trajectory in phase space (p, q) for the Kerr oscillator is analytically the same ellipse as for the harmonic oscillator

$$\frac{p^2}{p_0^2 + \omega_0^2 q_0^2} + \frac{\omega_0^2 q^2}{p_0^2 + \omega_0^2 q_0^2} = 1 \quad (18)$$

The only difference is that for the harmonic oscillator the phase point draws the ellipse with the frequency ω_0 , whereas for the Kerr oscillator with the frequency, $\Omega = \omega_0 [1 + \epsilon(p_0^2 + \omega_0^2 q_0^2)]$. The frequency Ω depends on the initial conditions, which is a feature typical of nonlinear conservative systems [143].

The set of equations (13)–(14) describes a conservative system. However, the effect of linear dissipation can be incorporated phenomenologically. Then, Eqs. (13)–(14) have the form

$$\frac{dq}{dt} = p[1 + \epsilon(p^2 + \omega_0^2 q^2)] - \gamma q \quad (19)$$

$$\frac{dp}{dt} = -\omega_0^2 q[1 + \epsilon(p^2 + \omega_0^2 q^2)] - \gamma p \quad (20)$$

where the terms γq and γp describe a loss mechanism, with the damping constant γ . The solution of the preceding equations is given by [142]

$$q(t) = e^{-\gamma t} \left(q_0 \cos N(t) + \frac{p_0}{\omega_0} \sin N(t) \right) \quad (21)$$

$$p(t) = e^{-\gamma t} (p_0 \cos N(t) - q_0 \omega_0 \sin N(t)) \quad (22)$$

where

$$N(t) = \omega_0 t + \frac{\epsilon \omega_0}{2\gamma} (p_0^2 + \omega_0^2 q_0^2) (1 - e^{-2\gamma t}) \quad (23)$$

If $\epsilon = 0$, the system (19)–(20) describes a damped linear oscillator governed by the equation

$$\frac{d^2 q}{dt^2} + 2\gamma \frac{dq}{dt} + (\omega_0^2 + \gamma^2) q = 0 \quad (24)$$

Generally, if Kerr systems are driven by external time-dependent forces, the equations of motion are nonintegrable and have to be studied numerically.

C. Dynamics of Linearly Coupled Kerr Oscillators

Let us consider a system of two classical oscillators with Kerr nonlinearity. Both oscillators interact with each other by way of a linear coupling; moreover, they are pumped by external time-dependent forces. The Hamiltonian for the system is given by

$$H = \sum_{i=1}^2 [H_i + \epsilon_i H_i^2 - q_i F_i(t)] - \alpha q_1 q_2 \quad (25)$$

where the Hamiltonian $H_i = \frac{1}{2}(p_i^2 + \omega_0^2 q_i^2)$ describes a simple harmonic oscillator with the frequency ω_0 . Moreover, $F_i(t) = A_i \cos \omega_i t$ is the time-dependent force, with the amplitude A_i and the frequency ω_i . The parameter of Kerr nonlinearity is denoted by ϵ_i . The interaction between the Kerr oscillators is governed by the term $\alpha q_1 q_2$, where α plays the role of an interaction parameter. The equations of motion for the system described by the Hamiltonian (25) are given by

$$\frac{dq_1}{dt} = p_1 [1 + \epsilon_1 (p_1^2 + \omega_0^2 q_1^2)] - \gamma_1 q_1 \quad (26)$$

$$\frac{dp_1}{dt} = -\omega_0^2 q_1 [1 + \epsilon_1 (p_1^2 + \omega_0^2 q_1^2)] + \alpha q_2 - \gamma_1 p_1 + A_1 \cos \omega_1 t \quad (27)$$

$$\frac{dq_2}{dt} = p_2 [1 + \epsilon_2 (p_2^2 + \omega_0^2 q_2^2)] - \gamma_2 q_2 \quad (28)$$

$$\frac{dp_2}{dt} = -\omega_0^2 q_2 [1 + \epsilon_2 (p_2^2 + \omega_0^2 q_2^2)] + \alpha q_1 - \gamma_2 p_2 + A_2 \cos \omega_2 t \quad (29)$$

where the terms $\gamma_i q_i$ and $\gamma_i p_i$ describe a loss mechanism. The loss mechanism has been incorporated phenomenologically. If the linear coupling parameter α is equal to zero, both anharmonic oscillators behave independently; that is, they do not interact with each other. Therefore, for $\alpha = 0$ the equations of motion (26)–(29) form two independent sets of equations. The equations of motion (26)–(29) give a four-dimensional nonautonomous system that can be easily autonomized [115] if we put $t = q_3$ in the functions $\cos \omega_i t$. Then, time becomes a dynamical variable and the fifth equation is given by

$$\frac{dq_3}{dt} = 1, \quad q_3(0) = 0 \quad (30)$$

In general, the system (26)–(30) is nonintegrable and its dynamics has to be studied numerically. We examined it with the help of a fourth-order Runge–Kutta

method. To calculate Lyapunov exponents, we used the procedure proposed by Wolf et al. [114]. The spectrum of the autonomized system (26)–(30) is denoted by the symbols $\{\lambda_1, \lambda_2, \lambda_3, \lambda_4, \lambda_5\}$.

1. Noninteracting Oscillators

Let us first consider the case of noninteracting oscillators that takes place when the interaction parameter α in Eqs. (26)–(29) is equal to zero. Then, the system (26)–(29) consists of two independent subsystems in the dynamical variables (q_1, p_1) and (q_2, p_2) . The parameters of the subsystems are $A_1 = A_2 = 200$, $\omega_0 = 1$, $\epsilon_1 = \epsilon_2 = 0.1$, $\gamma_1 = 0.05$, $\gamma_2 = 0.5$. The frequencies $\omega_{1,2}$ of the external driving forces vary in the range $0 < \omega_{1,2} < 3.2$. The autonomized spectrum of Lyapunov exponents $\{\lambda_1, \lambda_2, \lambda_3\}$ for the first oscillator *I* versus the frequency ω_1 is presented in Fig. 19a. We observe three types of spectra: $\{+, 0, -\}$, $\{0, 0, -\}$, and $\{0, -, -\}$. The first indicates a chaotic attractor; the second, a quasiperiodic orbit; and the third, a limit cycle. Therefore a change in the frequency ω_1 switches the chaotic oscillations (chaotic attractors) into nonchaotic oscillations (quasiperiodic orbits, limit cycles) and inversely. The autonomized spectrum of Lyapunov exponents for the second oscillator *II* versus the frequency ω_2 is shown in Fig. 19b. The difference between the two figures is essential. The chaotic regions in Fig. 19b do not appear at all because of the increase in damping in the system. The only attractors are limit cycles $\{0, -, -\}$. By way of an example, for identical frequencies $\omega_1 = \omega_2 = 0.55$, the Lyapunov spectra for the first and second oscillators are $\{0.08, 0.00, -0.23\}^I$ and $\{0.00, -0.55, -0.90\}^{II}$, respectively. The topology of the chaotic attractor in the phase space (q_1, p_1) is shown in Fig. 20a. The phase point starts from the initial conditions $q_{10} = 10$ and $p_{10} = 10$ and moves within the blackened area, which makes an attractor, after $t > 200$. In the phase plane (q_2, p_2) the phase point draws a limit cycle (Fig. 20b). The intricate structure of the limit cycle is related to multiperiodic oscillations of the system. The blackened areas at the top and bottom of the limit cycle have a periodic structure invisible in the scale of the phase portrait.

The single Kerr anharmonic oscillator has one more interesting feature. It is obvious that for $\epsilon_j = 0$ and $\gamma_j = 0$, the Kerr oscillator becomes a simple linear oscillator that in the case of a resonance $\omega_i = \omega_0$ manifests a primitive instability; in the phase space the phase point draws an expanding spiral. On adding the Kerr nonlinearity, the linear unstable system becomes highly chaotic. For example, putting $A_1 = 200$, $\omega_1 = \omega_0 = 1$, $\epsilon_1 = 0.1$ and $\gamma_1 = 0$, the spectrum of Lyapunov exponents for the first oscillator is $\{0.20, 0, -0.20\}^I$. However, the system does not remain chaotic if we add a small damping. For example, if $\gamma_1 = 0.05$, then the spectrum of Lyapunov exponents has the form $\{0.00, -0.03, -0.12\}^I$, which indicates a limit cycle.

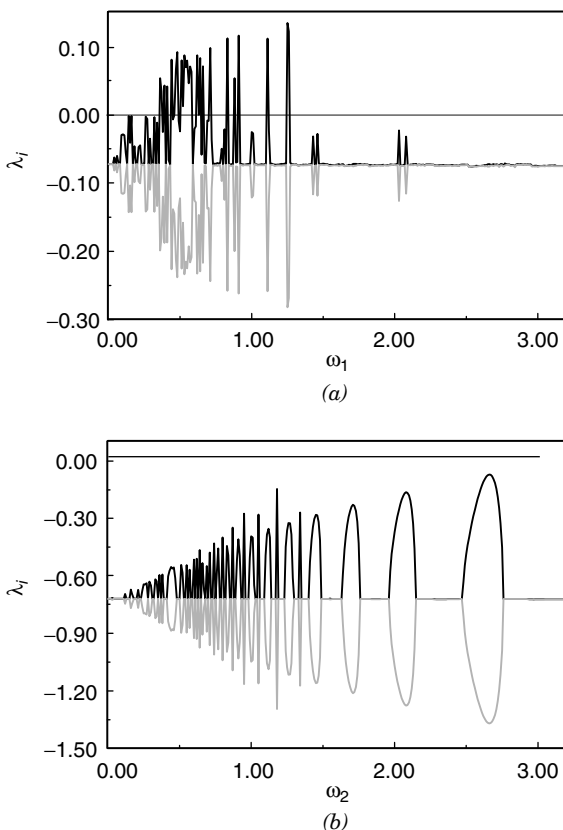


Figure 19. Spectra of Lyapunov exponents for the system (26)–(30) with $\alpha = 0$. The initial conditions are $q_{10} = 10, p_{10} = 10, q_{20} = 10,$ and $p_{20} = 10$. (a) Spectrum $\{\lambda_1, \lambda_2, \lambda_3\}^1$ for the first oscillator (I) versus the frequency ω_1 for $\omega_0 = 1, A_1 = 200, \gamma_1 = 0.05,$ and $\epsilon_1 = 0.1$. (b) The same for the second oscillator (II) with the parameters: $\omega_0 = 1, A_2 = 200, \gamma_2 = 0.5,$ and $\epsilon_2 = 0.1$.

2. Interacting Oscillators

If the interaction parameter α is switched on, the system of coupled oscillators (26)–(29) manifests a rich variety of spectacular behavior. Below, we concentrate on the most interesting ones. First, we answer the question as to how the attractors in Fig. 20 change when both oscillators interact with each other.

1. *The Case $A_1 = A_2, \gamma_1 < \gamma_2$.* The dynamics of the coupled oscillators is investigated for an interaction parameter α varying in the range $0 < \alpha < 1$. The

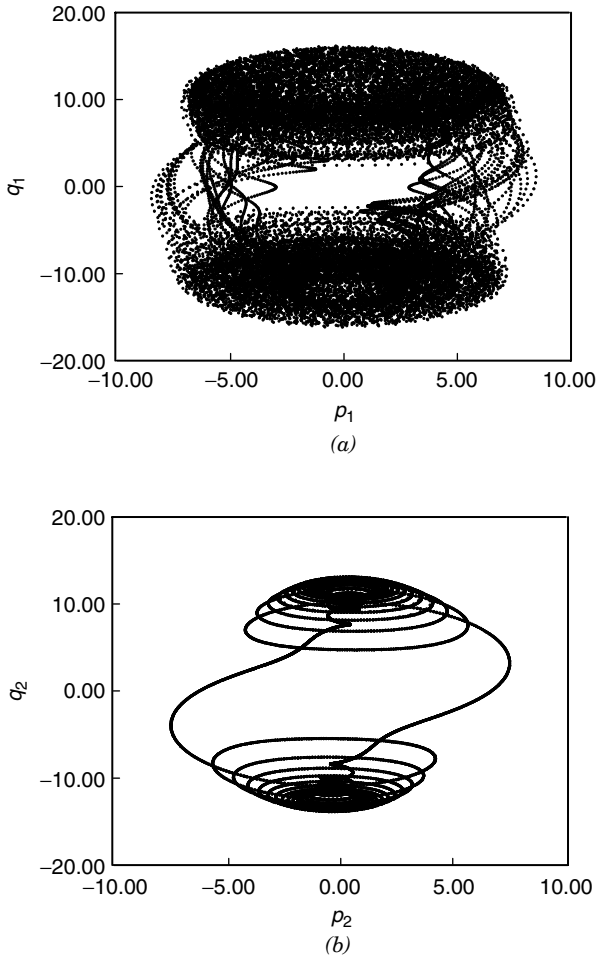


Figure 20. Phase portraits for the system (26)–(30) with $\alpha = 0$. The initial conditions are $q_{10} = 10, p_{10} = 10, q_{20} = 10,$ and $p_{20} = 10$. (a) Phase portrait (q_1, p_1) of the first oscillator for $A_1 = 200, \omega_0 = 1, \epsilon_1 = 0.1, \omega_1 = 0.55,$ and $\gamma_1 = 0.05$. (b) Phase portrait (q_2, p_2) of the second oscillator for $A_2 = 200, \omega_0 = 1, \epsilon_1 = 0.1, \omega_2 = 0.55,$ and $\gamma_1 = 0.5$.

joint autonomized spectrum of Lyapunov exponents $\{\lambda_1, \lambda_2, \lambda_3, \lambda_4, \lambda_5\}$ versus the interaction parameter α is shown in Fig. 21. The value $\alpha = 0$ is a limit value related to the dynamics of the uncoupled oscillators. This has already been done in Section III.C.1 In the region $0 < \alpha < 0.74$ the chaotic behavior of the coupled oscillator system predominates over the nonchaotic one; thus, for most values of

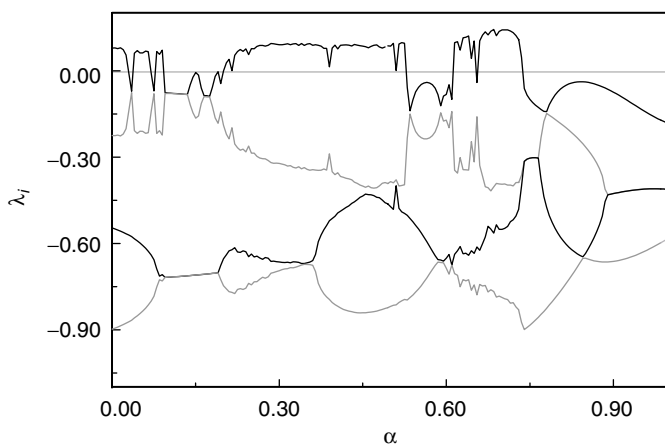


Figure 21. Spectrum of Lyapunov exponents $\{\lambda_1, \lambda_2, \lambda_3, \lambda_4, \lambda_5\}$ for the system (26)–(30) versus the interaction parameter α . The other parameters are $A_1 = A_2 = 200$, $\omega_0 = 1$, $\omega_1 = \omega_2 = 0.55$, $\epsilon_1 = \epsilon_2 = 0.1$, $\gamma_1 = 0.05$, and $\gamma_2 = 0.5$. The initial conditions are $q_{10} = 10$, $p_{10} = 10$, $q_{20} = 10$, and $p_{20} = 10$.

the parameter α , the maximal Lyapunov exponent is positive. For $0.68 < \alpha < 0.71$ we get the maximum chaos. For $\alpha > 0.74$ the system does not show chaotic behavior. Generally, the only spectra of Lyapunov exponents that appear in Fig. 21 are of types $\{+, 0, -, -, -\}$, $\{0, 0, -, -, -\}$, and $\{0, -, -, -, -\}$. These three types of spectra (for $\alpha > 0$) do not allow us to ascertain which of the two interacting oscillators is more (or less) chaotic than the other unless $\alpha = 0$. However, the dynamics of individual oscillators can be estimated with the help of the appropriate phase portraits. For example, if the interaction coupling is equal to $\alpha = 0.7$, the spectrum of Lyapunov exponents has the form $\{0.14, 0.00, -0.39, -0.55, -0.79\}$, and the appropriate phase portraits are as shown in Fig. 22. The attractors for the interacting oscillators shown in Fig. 22 are reminiscent of the attractors for noninteracting oscillators presented in Fig. 20. Let us note that the maximal Lyapunov exponent for the system of interacting oscillators, which is equal to $\lambda_1 = 0.14$, is greater than the maximal Lyapunov exponent for the uncoupled oscillators, which equals $\lambda_1 = 0.08$. Therefore, for $0.67 < \alpha < 0.72$, the coupled oscillators are more chaotic than their uncoupled version. However, as is seen from Fig. 21, this is not a rule. In the range $0.2 < \alpha < 0.5$ the values of the maximal Lyapunov exponent are of the rank ~ 0.08 , which corresponds to the value for uncoupled oscillators (a measure of chaos in the coupled and uncoupled oscillators is in practice the same). Therefore, the linear coupling here is relatively small in order to

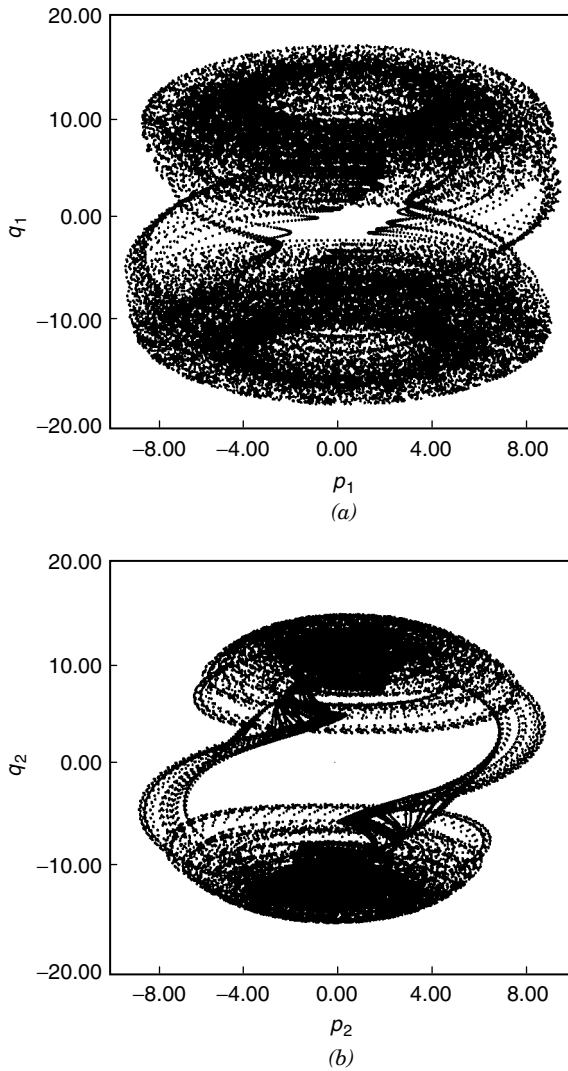


Figure 22. The same as in Fig. 20 but with the interaction parameter $\alpha = 0.7$.

additionally increase the instability of the system. Rather chaos flows from one oscillator to the other by the coupling term α .

2. *The Case* $A_1 = A$, $A_2 = 0$, $\gamma_1 = \gamma_2 = \gamma$. In what follows, we consider a simple version of the system (26)–(29), namely: both oscillators are equally

damped ($\gamma_1 = \gamma_2 = \gamma$) and only the first oscillator is externally pumped ($A_1 = A, A_2 = 0$). Therefore, the equations of motion are

$$\frac{dq_1}{dt} = p_1[1 + \epsilon(p_1^2 + \omega_0^2 q_1^2)] - \gamma q_1 \quad (31)$$

$$\frac{dp_1}{dt} = -\omega_0^2 q_1[1 + \epsilon(p_1^2 + \omega_0^2 q_1^2)] + \alpha q_2 - \gamma p_1 + A \cos \omega t \quad (32)$$

$$\frac{dq_2}{dt} = p_2[1 + \epsilon(p_2^2 + \omega_0^2 q_2^2)] - \gamma q_2 \quad (33)$$

$$\frac{dp_2}{dt} = -\omega_0^2 q_2[1 + \epsilon(p_2^2 + \omega_0^2 q_2^2)] + \alpha q_1 - \gamma p_2 \quad (34)$$

This system in its linear version (i.e., when $\epsilon = 0$) is a dynamical filter. Suppose that the oscillators interact with each other with the interaction parameter $\alpha = 0.9$. The frequency ω of the external driving field varies in the range $0 < \omega < 4.2$. The other parameters of the system are $A = 200$, $\omega_0 = 1$, $\epsilon = 0.1$, and $\gamma = 0.05$. The autonomized spectrum of Lyapunov exponents $\{\lambda_1, \lambda_2, \lambda_3, \lambda_4, \lambda_5\}$ versus the frequency ω is presented in Fig. 23. In the range $0 < \omega < 0.2$ the system does not exhibit chaotic oscillation. Here, the maximal Lyapunov exponent $\lambda_1 = 0$ and the spectrum is of the type $\{0, -, -, -, -\}$ (limit cycles). For example, for $\omega = 0.05$ we have $\{0.00, -0.07, -0.07, -0.07, -0.07\}$, and the limit cycles are shown in Fig. 24. The blackened areas in Fig. 24 have a periodic structure invisible in the scale applied. In the range $0.21 < \omega < 3.41$,

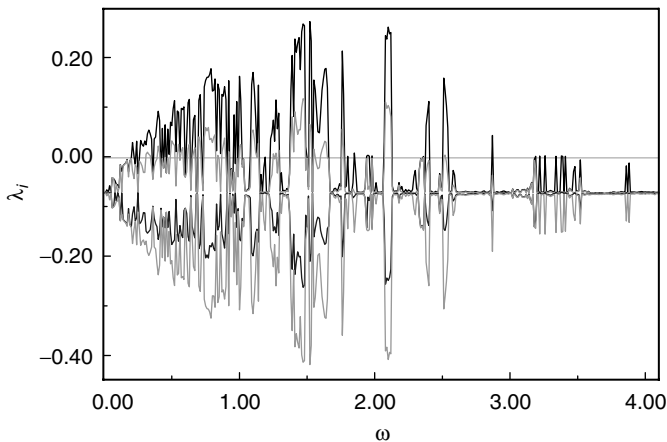


Figure 23. Spectrum of Lyapunov exponents $\{\lambda_1, \lambda_2, \lambda_3, \lambda_4, \lambda_5\}$ for the system (31)–(34) versus the pump frequency ω . The other parameters are $A = 200$, $\omega_0 = 1$, $\gamma = 0.05$, $\epsilon = 0.1$, and $\alpha = 0.9$. The initial conditions are $q_{10} = 10$, $p_{10} = 10$, $q_{20} = 10$, and $p_{20} = 10$.

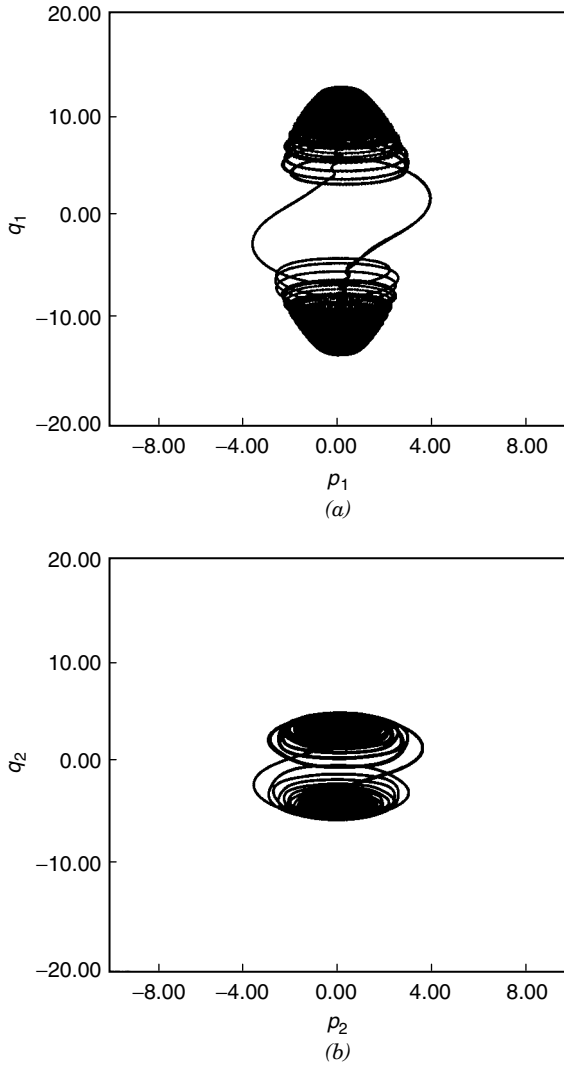


Figure 24. Phase portraits (q_1, p_1) and (q_2, p_2) for the system (31)-(34) with $\alpha = 0.9$. The other parameters are $A = 200, \omega_0 = 1, \epsilon = 0.1, \gamma = 0.05$, and $\omega = 0.05$. The initial conditions are the same as for Fig. 23. Limit cycles.

new types of spectra appear: $\{0, 0, -, -, -\}$, $\{+, 0, -, -, -\}$, and $\{+, +, 0, -, -\}$. The first indicate a quasiperiodic orbit; the second, a chaotic attractor, the third, a hyperchaotic attractor. Let us concentrate on the last and the most interesting case, with two positive Lyapunov exponents. The system reaches the

highest degree of hyperchaos for $\omega = 2.1$. Then, the spectrum is $\{0.26, 0.10, 0.00, -0.25, -0.41\}$, and the behavior of the phase point is presented in the phase diagrams in Fig. 25. Here, the phase point starts from the initial state $q_{10} = q_{20} = p_{10} = p_{20} = 10$ and moves into the hyperchaotic attractor after $t > 50$. For $\omega > 3.41$ the system behaves orderly.

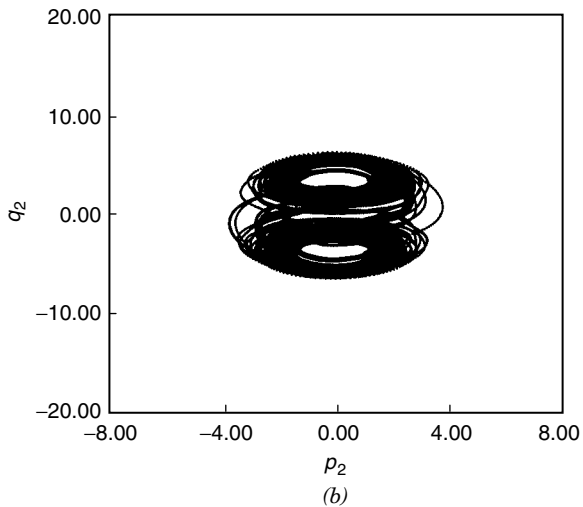
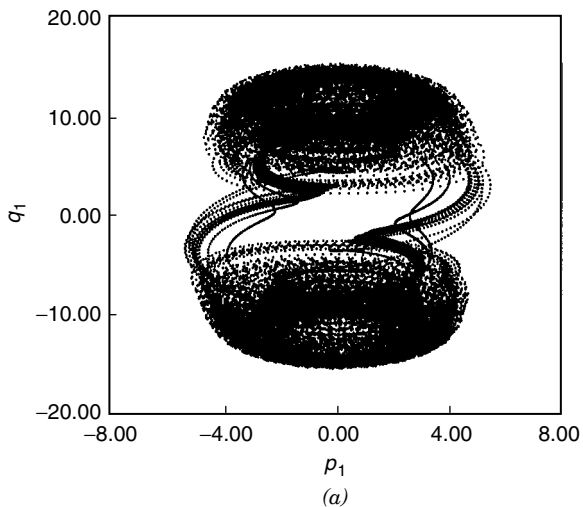


Figure 25. The same as in Fig. 24 but for $\omega = 2.1$. Hyperchaos.

The system (31)–(34) with $\epsilon = 0$ is a linear system with the normal frequencies $\Omega_1 = \sqrt{\omega_0^2 - \alpha}$ and $\Omega_2 = \sqrt{\omega_0^2 + \alpha}$. For $\omega_0 = 1$ and $\alpha = 0.9$, we have $\Omega_1 = 0.32$ and $\Omega_2 = 1.38$. It is known from linear dynamics that if $\Omega_1 > \omega > \Omega_2$, the steady-state amplitude of the first oscillator is greater than the steady-state amplitude of the second oscillator. If $\Omega_1 < \omega < \Omega_2$, we observe the inverse situation—the steady-state amplitude of the second oscillator is now greater than that of the first oscillator. This behavior is known as *dynamical filtering* of the signal $F(t) = A \cos \omega t$. The frequency range (Ω_1, Ω_2) is called the *charge-transfer band*, whereas Ω_1 and Ω_2 are the lower- and upper-band frequencies, respectively. The question is whether the filtering is, in a sense, also maintained in our nonlinear system. A detailed analysis shows that the vibrations of the first oscillator are always greater than the oscillations of the second oscillator, irrespective of the value of ω . This is also seen from the phase portraits in Figs. 24 and 25, which show that the *volume* of the attractor in the phase space (p_2, q_2) is always less than the attractors in the phase space (p_1, q_1) .

The linear version ($\epsilon = 0$) of the system (31)–(34) has one more interesting feature; namely, if $\gamma = 0$, $\omega = \omega_0$ and the following initial conditions are satisfied ($q_{10} = 0$, $p_{10} = 0$, $q_{20} = -A/\alpha$, $p_{20} = 0$), then the solutions of the linear equations of motion are $q_1(t) = 0$, $p_1(t) = 0$, $q_2(t) = (-A/\alpha) \cos \omega_0 t$ and $p_2(t) = (A\omega_0/\alpha) \sin \omega_0 t$. Therefore, the first oscillator remains in a state of rest and the second performs harmonic vibrations; such a system is frequently referred to as a *dynamical damper*. However, a nonlinear counterpart of the linear dynamical damper does not exist. For $\epsilon = 0.1$, $A = 9$, $\alpha = 0.9$, and $\omega = \omega_0 = 1$, the system behaves hyperchaotically. The spectrum of Lyapunov exponents is $\{0.68, 0.04, 0.00, -0.04, -0.68\}$.

Finally, let us briefly consider the dynamical properties of the system (31)–(34) without damping, that is, when $\gamma = 0$. The other parameters are $\omega_0 = 1$, $\alpha = 0.9$, and $A = 200$. The appropriate spectrum of Lyapunov exponents $\{\lambda_1, \lambda_2, \lambda_3, \lambda_4, \lambda_5\}$ versus the frequency $0 < \omega < 2$ is presented in Fig. 26. As is seen from Fig. 26, the system is completely hyperchaotic. Here, the only type of spectrum is $\{+, +, 0, -, -\}$. This type of spectrum is a case of the symmetric spectrum (the axis symmetry is the Lyapunov exponent $\lambda_3 = 0$).

3. Synchronization

In chaotic motion trajectories starting from insignificantly different initial conditions diverge from each other exponentially. The question is whether we can converge chaotic signals from two identically or slightly different subsystems, both starting from different initial conditions. This behavior is possible by linking them with a common signal and synchronizing both outputs. We show that two single Kerr oscillators are a convenient system for synchronization. According to the continuous feedback method [52,61,125,127], we consider two Kerr subsystems (oscillators) where one subsystem is called the

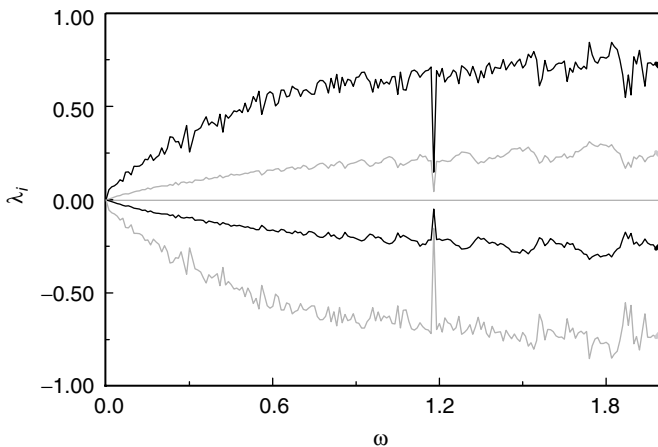


Figure 26. The same as in Fig. 23 but for $\gamma = 0$.

drive and the other the response. Both systems are coupled *unidirectionally* by a difference signal. The behavior of the response system depends only on the drive system, but not vice versa. The dynamics of our system is governed by the following set of equations:

$$\frac{dq_1}{dt} = p_1[+\epsilon_1(p_1^2 + \omega_0^2 q_1^2)] - \gamma_1 q_1 \tag{35}$$

$$\frac{dp_1}{dt} = -\omega_0^2 q_1[1 + \epsilon_1(p_1^2 + \omega_0^2 q_1^2)] - \gamma_1 p_1 + A_1 \cos \omega_1 t + S \tag{36}$$

$$\frac{dq_2}{dt} = p_2[1 + \epsilon_2(p_2^2 + \omega_0^2 q_2^2)] - \gamma_2 q_2 \tag{37}$$

$$\frac{dp_2}{dt} = -\omega_0^2 q_2[1 + \epsilon_2(p_2^2 + \omega_0^2 q_2^2)] - \gamma_2 p_2 + A_2 \cos \omega_2 t \tag{38}$$

where $S = \kappa(q_2 - q_1)$ is the difference signal and κ is the control parameter. As is seen, the second oscillator (drive) pumps a signal to the first oscillator (response) via the term S in Eq. (36). The synchronization of chaos (for a chosen parameter κ and the initial conditions $q_{10} \neq q_{20}$ and $p_{10} \neq p_{20}$) takes place if the chaotic trajectory $q_1 = q_1(t)$ of the response oscillator jumps after some time into the chaotic trajectory $q_2 = q_2(t)$ of the drive oscillator. The time needed to uniform chaotic motions of subsystems is called a *synchronization time*.

Let us consider the dynamics of synchronization for the system (35)–(38) with the parameters $A_1 = A_2 = 200$, $\omega_0 = 1$, $\omega_1 = \omega_2 = 0.55$, $\gamma_1 = \gamma_2 = 0.05$, and $\epsilon_1 = \epsilon_2 = 0.1$. The initial conditions for the drive and response systems are $(q_{10}, p_{10}) = (10, 10)$ and $(q_{20}, p_{20}) = (5, 5)$, respectively. For $\kappa = 0$ both systems draw different chaotic orbits. Figure 27 shows the measure of synchronization $\Delta_s = q_1(t) - q_2(t)$ versus time t for $\kappa = 0.33$. The appearance of the

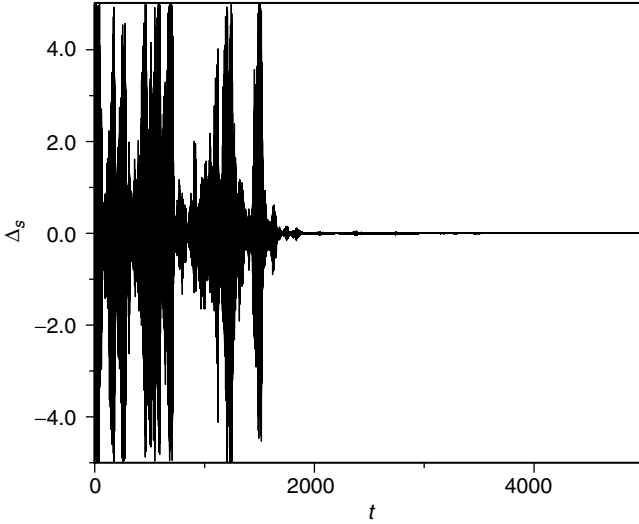


Figure 27. The time evolution of $\Delta_s = q_1 - q_2$ for $\kappa = 0.33$. The parameters and the initial conditions of the system (35)-(38) are $\omega_1 = \omega_2 = 0.55, A_1 = A_2 = 200, \omega_0 = 1, \epsilon_1 = \epsilon_2 = 0.1, \gamma_1 = \gamma_2 = 0.05, (p_{10}, q_{10}) = (10, 10),$ and $(p_{20}, q_{20}) = (5, 5)$.

straight line after $T_s \cong 2900$ clearly implies that both chaotic orbits have just been synchronized: $q_1(t) = q_2(t)$. The efficiency of the synchronization process depends on the parameter κ . This is illustrated in Fig. 28a, where the synchronization time T_s is presented as a function of the parameter κ . We observe four regions of synchronization: $0.28 < \kappa < 0.35, 0.42 < \kappa < 0.54, 0.77 < \kappa < 0.80,$ and $\kappa > 1.58$. In the other regions it is not possible to achieve the synchronization effect. The synchronization time takes the minimum value $T_s \cong 200$ for $\kappa > 1.59$.

In physical terms the unidirectional synchronization means that the drive oscillator plays the role of an external source. The situation is different if one considers the problem of a *mutual synchronization* of two oscillators, which we may assume to be identical in all respect except for the initial conditions: $q_{10} \neq q_{20}$ and $p_{10} \neq p_{20}$. Let us consider the following model of mutual synchronization

$$\frac{dq_1}{dt} = p_1[1 + \epsilon_1(p_1^2 + \omega_0^2 q_1^2)] - \gamma_1 q_1 \tag{39}$$

$$\frac{dp_1}{dt} = -\omega_0^2 q_1[1 + \epsilon_1(p_1^2 + \omega_0^2 q_1^2)] - \gamma_1 p_1 + A_1 \cos \omega_1 t + S \tag{40}$$

$$\frac{dq_2}{dt} = p_2[1 + \epsilon_2(p_2^2 + \omega_0^2 q_2^2)] - \gamma_2 q_2 \tag{41}$$

$$\frac{dp_2}{dt} = -\omega_0^2 q_2[1 + \epsilon_2(p_2^2 + \omega_0^2 q_2^2)] - \gamma_2 p_2 + A_2 \cos \omega_2 t - S \tag{42}$$

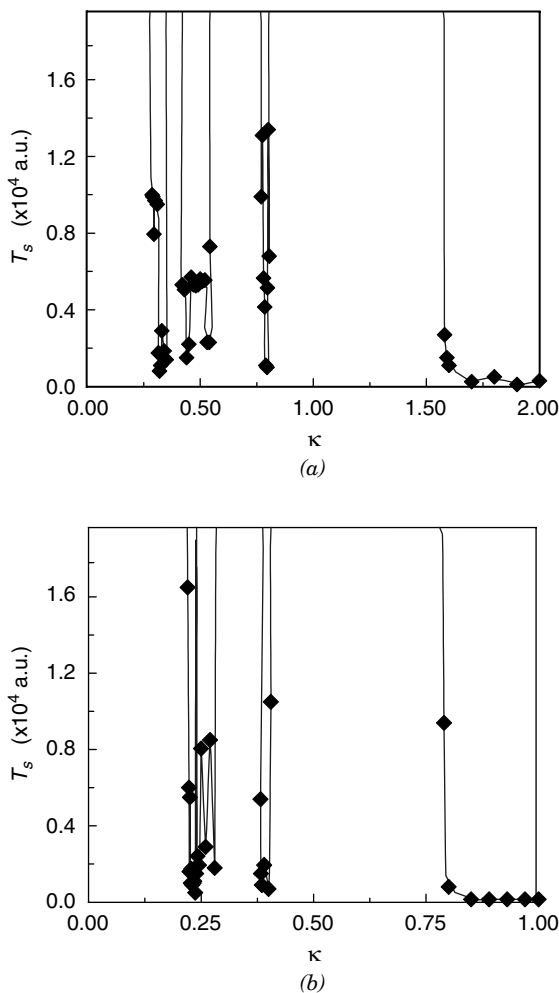


Figure 28. Synchronization time T_s versus κ . (a) for Eqs. (35)–(38); (b) for Eqs. (39)–(42). The parameters and the initial conditions are the same as for Fig. 27.

where $S = \kappa(q_2 - q_1)$. The system is similar to that governed by Eqs. (26)–(29). The equations of motion (39)–(42) can be derived from the Hamiltonian (25) if, instead of $\alpha q_1 q_2$, we put $0.5\kappa(q_1 - q_2)^2$. The values of the parameters and the initial conditions for the model of mutual synchronization are the same as for the unidirectional model. Synchronization takes place in the ranges $0.22 < \kappa < 0.27$, $0.38 < \kappa < 0.41$ and $\kappa > 0.79$, as is shown in Fig. 28b. For $\kappa > 0.80$ we obtain the minimum value of $T_s \cong 150$

It is interesting to note that the regions of unidirectional and mutual synchronization do not overlap. In both cases we have the critical value of κ (1.59, unidirectional synchronization; 0.80, mutual synchronization), after which the coupling is strong enough to maximize the process of synchronization.

4. Chaotic Beats

Let us now concentrate on the problem of beats generated by the system (26)–(29) without a loss mechanism ($\gamma_1 = \gamma_2 = 0$). For $\gamma_1 = \gamma_2 = 0$, and $\alpha = 0$, the dynamics of the system (26)–(29) is reduced to two noninteracting Kerr subsystems:

$$\frac{dq_j}{dt} = p_j[1 + \epsilon_j(p_j^2 + \omega_0^2 q_j^2)] \quad (43)$$

$$\frac{dp_j}{dt} = -\omega_0^2 q_j[1 + \epsilon_j(p_j^2 + \omega_0^2 q_j^2)] + A_j \cos \omega_j t, \quad j = 1, 2 \quad (44)$$

These Kerr oscillators, with $\epsilon_1 = \epsilon_2 = 0$, are linear subsystems that in the case of resonance ($\omega = \omega_1 = \omega_2$) exhibit a common instability—the solutions of Eqs. (43) and (44) for $t \rightarrow \infty$ grow linearly without bound. This resonance instability of our linear subsystems vanishes for $\epsilon_1 \neq 0$ and $\epsilon_2 \neq 0$. The subsystems become stable but only for small values of ϵ_1 and ϵ_2 . For example, beats generated by the first oscillator for $\epsilon_1 = 10^{-9}$, $A_1 = 200$, and $\omega_0 = \omega_1 = 1$ are illustrated in Fig. 29a, and the appearing beats originate from the Kerr nonlinearity.

Beats generated by the second oscillator for $\epsilon_2 = 10^{-9}$, $A_2 = 200$, $\omega_0 = 1$, and $\omega_2 = 1.05$ are shown in Fig. 29b. The Lyapunov analysis of beats presented in Fig. 29 leads to the conclusion that the beats have a quasiperiodic nature, or, as we frequently say, they are almost periodic solutions and our system can be treated as a nearly linear system [143]. The structure of beats in the coupled system (26)–(29) is much more intricate than for the individual noninteracting subsystems (43)–(44), where the beats are quasiperiodic functions. Let us suppose that the individual noninteracting oscillators ($\alpha = 0$) behave as presented in Fig. 29 and answer the question as to how the structure of beats in both figures change when the oscillators interact with each other ($\alpha \neq 0$), that is, how the occurrence of beats in the coupled oscillators depends on the selected value of α . Numerical calculations show that the coupled system generates distinct beats if $\alpha < 0.3$. Let us now have a look at the Lyapunov analysis of beats. The autonomized spectrum of Lyapunov exponents for the system (26)–(29) versus the coupling parameter ($0 < \alpha < 0.16$) is presented in Fig. 30. As is seen, the most spectacular behavior of the system is observed for $0.01 < \alpha < 0.13$. In this range our system generates beats and behaves hyperchaotically. The magnitude of chaos depends on the value of the coupling parameter α . The highest degree

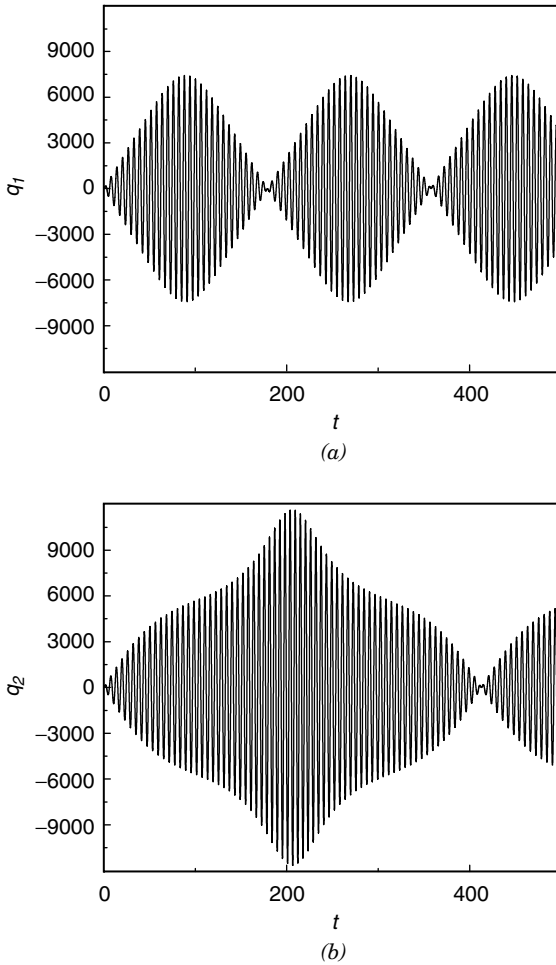


Figure 29. Evolution of q_1 and q_2 versus t for Eqs. (26)–(29) with $\alpha = 0$. The initial conditions are $q_{10} = 10, p_{10} = 10, q_{20} = 10$, and $p_{20} = 10$. The other parameters are $A_1 = A_2 = 200, \gamma_1 = \gamma_2 = 0, \epsilon_1 = \epsilon_2 = 10^{-9}$, and $\omega_0 = \omega_1 = 1$ (a), $\omega_0 = 1, \omega_2 = 1.05$ (b).

of hyperchaos is achieved at $\alpha = 0.04$, and the spectrum of the Lyapunov exponents is given by the following set $\{0.013, 0.003, 0.000, -0.003, -0.013\}$. The beats with chaotic envelopes in the q_1 -component are shown in Fig. 31a. The envelope function is very sensitive to the interaction parameter α . A small change in α , for example, from $\alpha = 0.04$ to $\alpha = 0.05$ drastically changes the shape of the envelope function (Fig. 31a,b), leaving the basic frequency of oscillations almost unchanged (Fig. 31, window). As seen in Fig. 31, the

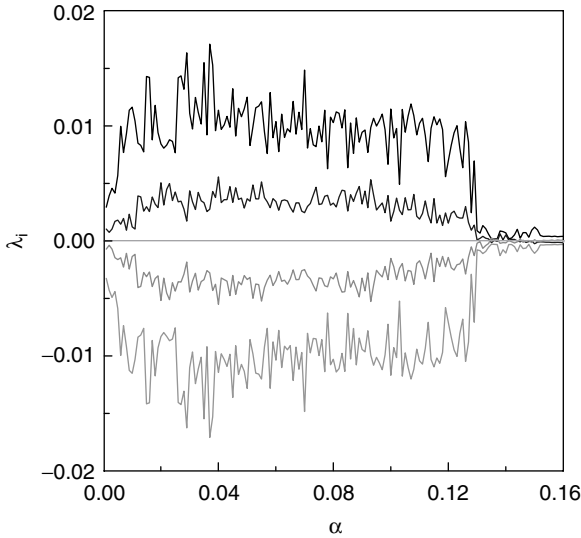


Figure 30. Spectra of Lyapunov exponents $\{\lambda_1, \lambda_2, \lambda_3, \lambda_4, \lambda_5\}$ for the system (26)–(29) versus the coupling constant α . The other parameters are $A_1 = A_2 = 200, \gamma_1 = \gamma_2 = 0, \omega_0 = 1, \omega_1 = 1, \omega_2 = 1.05$, and $\epsilon_1 = \epsilon_2 = 10^{-9}$. The initial conditions are $q_{10} = 10, q_{20} = 10, p_{10} = 10$, and $p_{20} = 10$.

envelope functions can be drawn as smooth functions, in contradistinction to the envelopes of beats generated stochastically [144,145]. For $\alpha > 0.16$ the beats lose their chaotic behavior and for $\alpha > 0.4$, the beats vanish completely.

It is interesting that envelope functions can also behave as multiperiod oscillations. This takes place if we take into account small damping. By way of an example, for the damping constant $\gamma_1 = \gamma_2 = 0.1$, the envelope function has a feature of two period doubling oscillations.

5. Final Remarks

The dynamics of two linear coupled Kerr oscillators strongly depends on the value of the interaction parameter α , frequency of pumping fields ω_j , and the damping constants γ_j . If the oscillators are coupled, both undergo a homogenization regarding the nature of their motion; either both are chaotic, or both are ordered, as is obvious from the phase graphs. For some parameters chaotic signals generated by the Kerr oscillators can be synchronized. Both unidirectional and mutual synchronization have been studied. The phenomenon of beats appears in linear and nonlinear systems whenever an impressed frequency is close to a natural frequency of a linear system or whenever two slightly different frequencies are impressed on a system regardless of what its natural frequencies

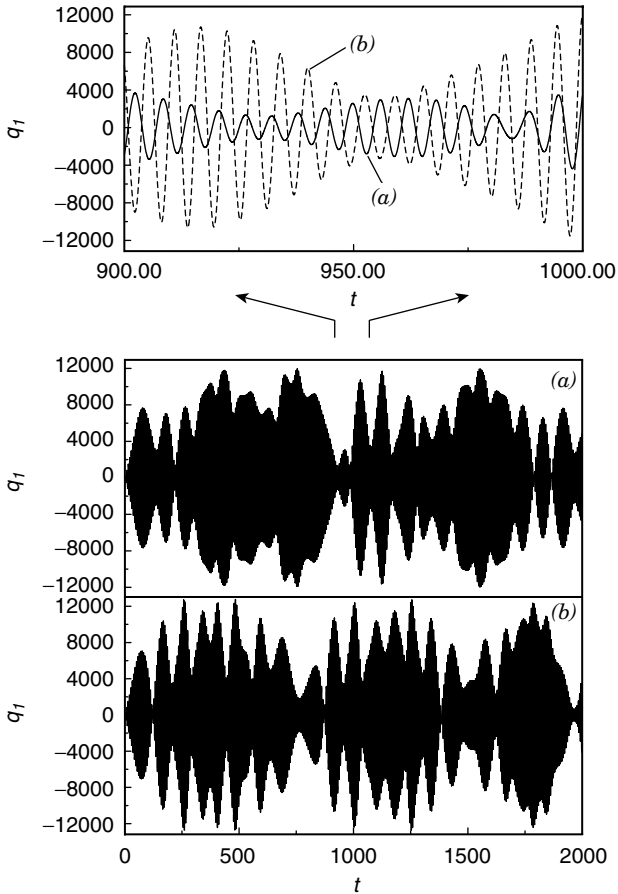


Figure 31. Evolution of $q_1(t)$ versus for Eqs. (26)-(29) from the initial conditions $q_{10} = 10, p_{10} = 10, q_{20} = 10,$ and $p_{20} = 10$ for (a) $\alpha = 0.04,$ (b) $\alpha = 0.05.$ The other parameters are $A_1 = A_2 = 200, \gamma_1 = \gamma_2 = 0, \omega_0 = 1, \omega_1 = 1, \omega_2 = 1.05,$ and $\epsilon_1 = \epsilon_2 = 10^{-9}.$

may be. For the small parameters of nonlinearity $\epsilon = 10^{-9},$ the quasiperiodic beats in uncoupled Kerr oscillators become beats with chaotic envelopes if the Kerr oscillators are linearly coupled. A small change in the interaction parameter rapidly changes the shape of the envelopes, whereas the basic frequencies of vibrations remains practically unchanged. Therefore the coupled oscillators can be used as a source of signals with chaotic envelopes and stable fundamental frequency. The appropriate materials useful for the generation of beats with chaotic envelopes could be optical systems consisting of a pair of

coupled Kerr fibers [138,139,146]. Since the pioneering work by Jensen [136], twin-core nonlinear fibers (so-called couplers) have been one of the highest-priority topics of fiberoptic research. The couplers are expected to find important applications as all-optical switches [147] in photonics, for example. Another interesting problem connected with optical application to secure communication is synchronization of coupled systems [148,149].

D. Dynamics of Nonlinearly Coupled Kerr Oscillators

Let us now consider a system of two nonlinearly coupled Kerr oscillators. Now, we write the Hamiltonian (25) in the form

$$H = \sum_{i=1}^2 [H_i + \epsilon_i H_i^2 - q_i F_i(t)] + 2\epsilon_{12} H_1 H_2 \tag{45}$$

where ϵ_{12} the intermodal coupling constant. The autonomized equations of motion for the Hamiltonian (45) have the following form:

$$\frac{dq_1}{dt} = p_1 [1 + \epsilon_{11}(p_1^2 + \omega_0^2 q_1^2) + \epsilon_{12}(p_2^2 + \omega_0^2 q_2^2)] - \gamma_1 q_1 \tag{46}$$

$$\begin{aligned} \frac{dp_1}{dt} = & -\omega_1^2 q_1 [1 + \epsilon_{11}(p_1^2 + \omega_0^2 q_1^2) + \epsilon_{12}(p_2^2 + \omega_0^2 q_2^2)] \\ & - \gamma_1 p_1 + A_1 \cos \omega_1 t \end{aligned} \tag{47}$$

$$\frac{dq_2}{dt} = p_2 [1 + \epsilon_{22}(p_2^2 + \omega_0^2 q_2^2) + \epsilon_{12}(p_1^2 + \omega_0^2 q_1^2)] - \gamma_2 q_2 \tag{48}$$

$$\begin{aligned} \frac{dp_2}{dt} = & -\omega_2^2 q_2 [1 + \epsilon_{22}(p_2^2 + \omega_0^2 q_2^2) + \epsilon_{12}(p_1^2 + \omega_0^2 q_1^2)] \\ & - \gamma_2 p_2 + A_2 \cos \omega_2 t \end{aligned} \tag{49}$$

$$\frac{dq_3}{dt} = 1, \quad q_3(0) = 0 \tag{50}$$

Let us emphasize that if $A_j = 0$, the set of equations (46)–(50) is integrable and has a relatively simple analytic solution. If the initial state of the system is determined by the initial conditions $q_j(0) = q_{j0}$ i $p_j(0) = p_{j0}$, the analytic solution is given by [110]

$$q_j(t) = e^{-\gamma_j t} \left(q_{j0} \cos E_j(t) + \frac{p_{j0}}{\omega_j} \sin E_j(t) \right) \tag{51}$$

$$p_j(t) = e^{-\gamma_j t} (p_{j0} \cos E_j(t) - \omega_j q_{j0} \sin E_j(t)), \quad j = 1, 2 \tag{52}$$

where

$$E_1(t) = \omega_0 t + \frac{\epsilon_1 \omega_0}{\gamma_1} H_{10}(1 - e^{-2\gamma_1 t}) + \frac{\epsilon_{12} \omega_0}{\gamma_2} H_{20}(1 - e^{-2\gamma_2 t}) \quad (53)$$

$$E_2(t) = \omega_0 t + \frac{\epsilon_2 \omega_0}{\gamma_2} H_{20}(1 - e^{-2\gamma_2 t}) + \frac{\epsilon_{12} \omega_0}{\gamma_1} H_{10}(1 - e^{-2\gamma_1 t}) \quad (54)$$

$$H_{j0} = \frac{p_{j0}^2}{2} + \frac{\omega_0^2 q_{j0}^2}{2}, \quad j = 1, 2 \quad (55)$$

The system (46)–(50) is examined numerically with the following parameters: $A_1 = A_2 = 200$, $\omega_0 = 1$, $\epsilon_1 = \epsilon_2 = 0.1$, $\gamma_1 = 0.05$, $\gamma_2 = 0.5$. The frequencies $\omega_{1,2}$ of the external driving forces and the cross interaction Kerr constant ϵ_{12} vary in the range $0 < \omega_{1,2} < 3$ and $0 < \epsilon_{12} < 1.5$, respectively. Therefore we study the dynamics of two nonlinearly coupled oscillators, I and II, which differ only in the value of the damping constants γ_1 and γ_2 .

1. Noninteracting Oscillators

The case of noninteracting oscillators takes place when the coupling constant ϵ_{12} is equal to zero. Then, the systems (46)–(50) with $\epsilon_{12} = 0$ and (26)–(29) with $\alpha = 0$ are identical, and their dynamics are considered in Section III.C.1.

2. Interacting Oscillators

Let us now consider the behavior of the system when the Kerr coupling constant is switched on ($\epsilon_{12} \neq 0$). For brevity and clarity, we restrict our discussion to the question of how the attractors in Fig. 20 change when both oscillators interact with each other. To answer this question, let us have a look at the joint auto-nomized spectrum of Lyapunov exponents for the two oscillators $\{\lambda_1, \lambda_2, \lambda_3, \lambda_4, \lambda_5\}$ versus the interaction parameter $0 < \epsilon_{12} < 0.7$. The spectrum is seen in Fig. 32 and describes the dynamical properties of our oscillators in a global sense. The dynamics of individual oscillators can be glimpsed at the appropriate phase portraits. Let us now fix our attention on a detailed analysis of Fig. 32. For the limit value $\epsilon_{12} = 0$, the dynamics of the uncoupled oscillators has already been presented in Fig. 20. In the case of very weak interaction $0 < \epsilon_{12} < 0.0005$, the system of coupled oscillators manifests chaotic behavior. For $\epsilon_{12} = 0.0005$ we obtain the spectrum $\{0.06, 0.00, -0.21, -0.54, -0.89\}$. It is interesting to note that the maximal Lyapunov exponent $\lambda_1 = 0.08$ for the system of noninteracting oscillators ($\epsilon_{12} = 0$) is greater than the maximal Lyapunov exponent $\lambda_1 = 0.06$ for the coupled system with the parameter $\epsilon_{12} = 0.0005$. Therefore, in this case, the uncoupled system is more chaotic than the coupled system. A further increase in the interacting parameter ϵ_{12} leads to the disappearance of chaos. In the region $0.0005 < \epsilon_{12} < 0.15$ the oscillators behave orderly and nonchaotically. By way of example, for $\epsilon_{12} = 0.1$, all the values of

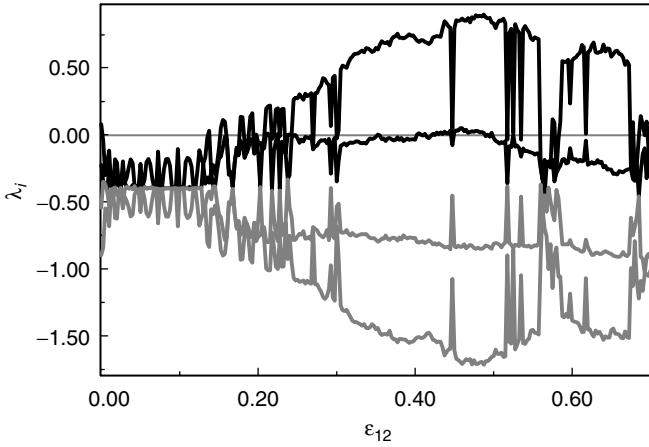


Figure 32. Spectrum of Lyapunov exponents $\{\lambda_1, \lambda_2, \lambda_3, \lambda_4, \lambda_5\}$ for the system (46)–(50) versus the Kerr coupling constant ϵ_{12} . The other parameters are $\omega_0 = 1, \omega_1 = \omega_2 = 0.55, A_1 = A_2 = 200$, and $\epsilon_1 = \epsilon_2 = 0.1$. The initial conditions are $q_{10} = 10, p_{10} = 10, q_{20} = 10$, and $p_{20} = 10$.

Lyapunov exponents are nonpositive: $\{0.00, -0.12, -0.26, -0.53, -0.68\}$. In this case the appropriate limit cycles are shown in Fig. 33a,b. The intricate structure of the limit cycles is reminiscent of the structure seen in Fig. 20. The blackened areas in Fig. 33 contain some pattern structure invisible in the scale used. As we see from Fig. 32, the situation changes in the region $0.15 < \epsilon_{12} < 0.43$. Chaotic behavior of the system predominates over nonchaotic behavior—for most values of the parameter ϵ_{12} , one Lyapunov exponent is positive. The most spectacular behavior of the coupled oscillators is observed in the region $0.43 < \epsilon_{12} < 0.49$. Here, two positive Lyapunov exponents in the spectrum indicate hyperchaotic behavior of the system. The highest degree of hyperchaos is achieved by the system at $\epsilon_{12} = 0.46$. The spectrum of the Lyapunov exponents is given by the set $\{0.87, 0.05, 0.00, -0.83, -1.71\}$, pointing to the existence of an hyperchaotic attractor. Its topology in the phase portraits (q_1, p_1) and (q_2, p_2) is shown in Fig. 34a,b. Precisely, in the phase portraits the system initially manifests a transient behavior but then (for $t > 500$) settles into a hyperchaotic attractor.

For $\epsilon_{12} \geq 0.49$ we observe a reduction of hyperchaos to chaos. Generally, in the region $0.49 \leq \epsilon_{12} \leq 0.75$ chaos dominates order and is maximal for the value $\epsilon_{12} = 0.63$, and the spectrum is $\{0.67, 0.00, -0.20, -0.90, -1.48\}$. Spectacular chaotic attractors appear for $\epsilon_{12} = 0.7$. Their phase portraits are presented in Fig. 35, where both attractors make impressions of spread limit cycles, as

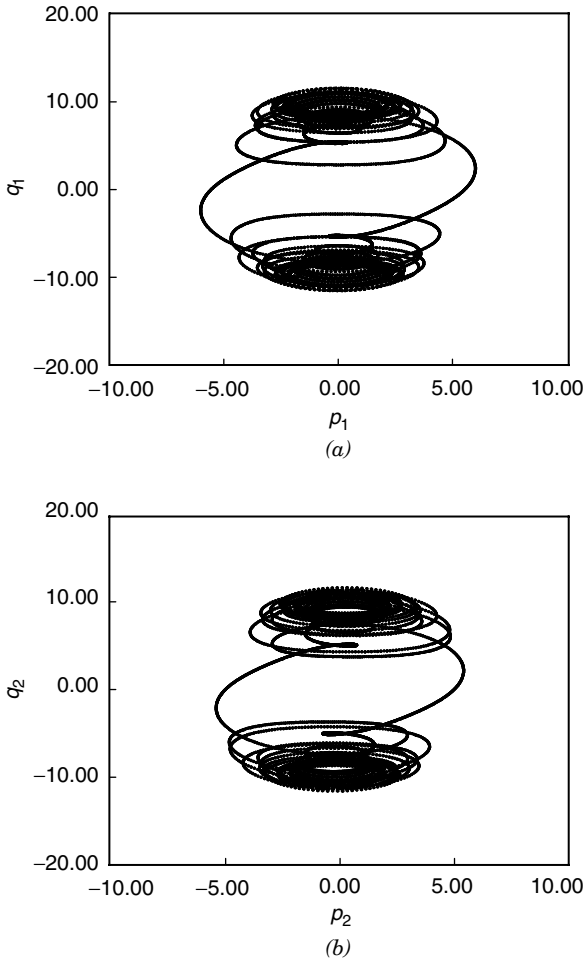


Figure 33. Phase portraits for the system (46)–(50) for $\epsilon_{12} = 0.1$ with the initial conditions $q_{10} = 10, p_{10} = 10, q_{20} = 10,$ and $p_{20} = 10$: (a) phase portrait (q_1, p_1) of the first oscillator for $A_1 = 200, \omega_0 = 1, \epsilon_1 = 0.1, \omega_1 = 0.55,$ and $\gamma_2 = 0.05$; (b) phase portrait (q_2, p_2) of the second oscillator for $A_2 = 200, \omega_0 = 1, \epsilon_2 = 0.1, \omega_2 = 0.55,$ and $\gamma_2 = 0.5$. Order.

chaos is relatively small here. The spectrum of Lyapunov exponents is $\{0.06, 0.00, -0.31, -0.92, -1.01\}$.

3. Final Remarks

The emergence of order and chaos in the system of two oscillators depends on the value of the Kerr coupling constant ϵ_{12} . For the fixed parameters of damping

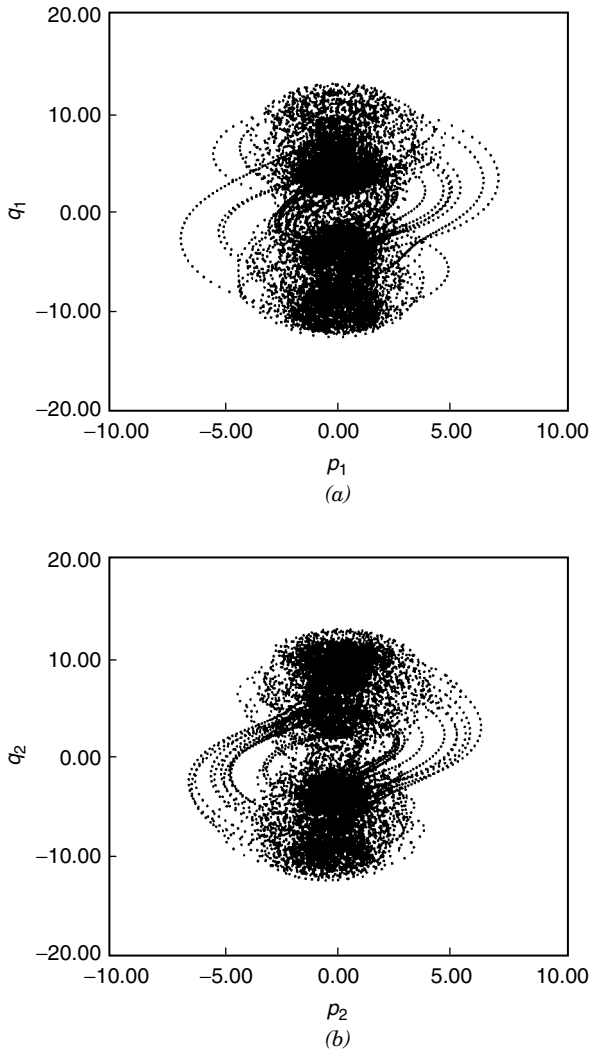


Figure 34. The same as in Fig. 33 but with $\epsilon_{12} = 0.46$. Hyperchaos.

γ_i , the sum of all exponents in the Lyapunov spectrum is not an invariant of the parameter ϵ_{12} . For the noninteracting oscillators ($\epsilon_{12} = 0$), the sum is equal to $\sum_{i=1}^5 \lambda_i = -1.60$ and tends to the value $\sum_{i=1}^5 \lambda_i = -2.25$ if $\epsilon_{12} \rightarrow 0.7$. Therefore we can say that the coupling term with ϵ_{12} in the equations of motion has an attribute of damping. These negative values result from nonconservation of volume in phase space (for conservative systems, the sum of Lyapunov

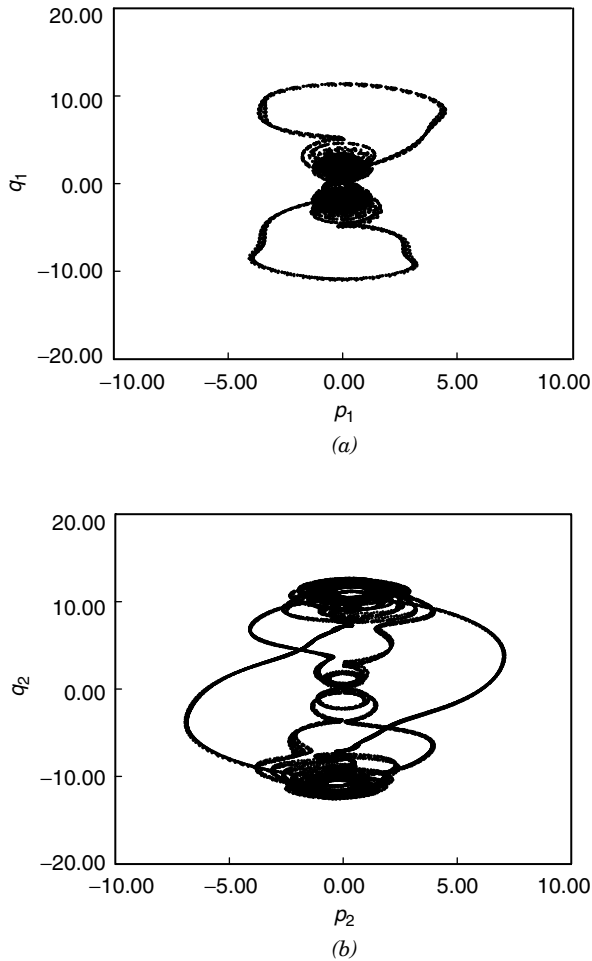


Figure 35. The same as in Fig. 33 but for with $\epsilon_{12} = 0.7$. Weak chaos.

exponents equals zero). Obviously, even if the volume of the system is suppressed, this does not mean that its length is equally suppressed in *all* directions. Some directions are stretched. In the direction of stretching we observe only an exponential separation of the trajectories, namely, chaotic or hyperchaotic behavior of the system. Finally, let us emphasize that the appropriate media for the experimental studies of chaotic behavior generated by Kerr nonlinearities could be optical fibers. The appearance of chaotic output signals generated by Kerr media means that the signals are unstable. The instability depends on

the value of the coupling constant ϵ_{12} . Therefore, by changing the value of the coupling constant, we can turn the output chaotic signals into the periodic ones and vice versa. Promising materials for the implementation of nonlinear Kerr oscillators also seem to be some organic polymers [150].

IV. QUANTUM CHAOS

The modifications introduced by quantum mechanics into the dynamics of classical systems that manifest deterministic chaotic behavior are frequently referred to collectively as “quantum chaos” [4,6,13,151–161]. It is rather conceded that quantization drastically modifies classically chaotic behavior. For example, suppression of chaos to quasiperiodicity is observed in the quantum kicked rotator, whose classical counterpart behaves chaotically [6,151,152]. In the system of a hydrogen atom in a microwave field, quantum effects suppress diffusive ionization by the mechanism of quantum localization [153,154]. Certain manifestations of chaos also become apparent in quantum optics [84, 162–167]. It seems that Wigner’s formulation of quantum mechanics offers the simplest comparison between quantum and classical chaos in contradistinction to the conventional procedure. The conventional way is to study how a wavepacket initially fixed around a certain position q and momentum p follows the appropriate classical trajectory. However, this involves a disadvantage. Specifically, the wavepacket spreads in the course of time and is no longer sharply fixed around a particular position and momentum, rendering dubious the comparison with the respective classical trajectory. To avoid this spreading problem, we can make use of the so-called Wigner symbols, which are a quantum generalization of classical variables. For example, we can compare the time evolution of the Wigner symbols for the position \hat{q} and momentum \hat{p} operators with the classical evolution of the position q and momentum p , respectively. Generally, Wigner’s formulation of quantum mechanics leads to a c -number representation of the density matrix, that is, to the quantum analog of a classical probability density in (p, q) space. In quantum optics three kinds of c -number functions are the most popular, the P representation, the Q function, and the Wigner function W [168]. All these three functions are defined in $(\alpha = p + iq, \alpha^* = p - iq)$ space instead of in (p, q) space. This is due to the coherent state technique. The P representation is related to normal ordering of the creation \hat{a}^\dagger and annihilation \hat{a} operators, the Q function is related to antinormal ordering of the operators, and the Wigner function W is related to symmetric (Weyl) ordering. The c -number approach makes it possible to treat quantum systems in a “classical way,” including all their quantum features and contrasting the quantum and classical dynamics within the framework of a phase picture. The equations for the Wigner-like functions P and Q belong to the class of generalized Fokker–Planck equations whose solutions are known only for some

simple optical models. The Wigner approach can also be used to study both “kicked” dynamics (i.e., a quantum map) and a continuous flow. Kicked models are easier to analyze numerically than continuous models but are more difficult to verify practically. On the other hand, continuous models seem to be mathematically more cumbersome, resembling the complexity of hydrodynamical systems. In the latter case we usually make some truncations leading to a set of ordinary differential equations. Historically, for the first time in the treatment of classical dynamical systems, a truncation method was used by Lorenz [2]. A similar truncation method can be used for generalized Fokker–Planck equations if we note that these equations generate a hierarchic and infinite set of ordinary differential equations for statistical cumulants [169–171]. The first truncation always leads to equations having the form of classical equations of motion. The second truncation plays the role of the first quantum correction, and so on. The cumulant method has also been applied to the study of some aspects of chaos in classical and quantum mechanics [173,174] and in quantum optics [165,166,171,172]. To identify chaotic behavior of a classical dynamical system, it suffices to use the maximal Lyapunov exponent. A quantum analog of the Lyapunov exponent involving the Q function has been proposed by Toda and Ikeda [175]. However, as we have already mentioned, the equation for the $Q(P, W)$ function is mathematically cumbersome, and its analytical solution is unknown for most nonlinear systems. This poses additional difficulties when it comes to calculate the Lyapunov exponents. However, this problem can be solved indirectly and approximately by finite cumulant expansion [165], enabling us to use the classical calculation method of Lyapunov exponents for equations with statistical cumulants.

A. Chaos in a Kerr Oscillator

We write the Hamiltonian in the form

$$\hat{H} = \hat{H}_1 + \hat{H}_2 + \hat{H}_3 \quad (56)$$

where

$$\hat{H}_1 = \hbar\omega\hat{a}^\dagger\hat{a} + \frac{\hbar\chi}{2}\hat{a}^{\dagger 2}\hat{a}^2 \quad (57)$$

$$\hat{H}_2 = i\hbar F(\hat{a}^\dagger - \hat{a}) \quad (58)$$

$$\hat{H}_3 = \hbar \sum_j \Omega_j \hat{b}_j^\dagger \hat{b}_j + \hbar \sum_j (K_j \hat{b}_j \hat{a}^\dagger + K_j^* \hat{b}_j^\dagger \hat{a}) \quad (59)$$

In the single-mode Hamiltonian \hat{H}_1 , the quantities \hat{a} (\hat{a}^\dagger) are the photon annihilation (creation) operators, respectively; ω is the frequency of the

harmonic oscillator, and χ is the anharmonicity parameter. The Hamiltonian \hat{H}_2 describes the interaction between the classical external driving field F and the single-mode field. The loss mechanism is described by the coupling to a heat bath governed by the reservoir Hamiltonian \hat{H}_3 . Here, the $(\hat{b}_j)\hat{b}_j^\dagger$ are the boson annihilation (creation) operators of the reservoir. The frequencies of the reservoir modes are denoted by Ω_j . The quantities K_j are the coupling constants between the optical and reservoir modes. On eliminating the reservoir operators, we obtain the master equation for the density operator $\hat{\rho}$ in the following form:

$$\frac{\partial \hat{\rho}}{\partial t} = \frac{-i}{\hbar} [\hat{H}_1 + \hat{H}_2, \hat{\rho}] + L_{ir}[\hat{\rho}] \quad (60)$$

The irreversible term $L_{ir}[\hat{\rho}]$ describes damping and has the following form:

$$\begin{aligned} L_{ir}[\hat{\rho}] = & \frac{\Gamma}{2} (2\hat{a}\hat{\rho}\hat{a}^\dagger - \hat{a}^\dagger\hat{a}\hat{\rho} - \hat{\rho}\hat{a}^\dagger\hat{a}) \\ & + \Gamma \langle n \rangle (\hat{a}^\dagger\hat{\rho}\hat{a} + \hat{a}\hat{\rho}\hat{a}^\dagger - \hat{a}^\dagger\hat{a}\hat{\rho} - \hat{\rho}\hat{a}\hat{a}^\dagger) \end{aligned} \quad (61)$$

The parameter Γ is the damping constant, and $\langle n \rangle$ is the mean number of reservoir photons. The quantum theory of damping assumes that the reservoir spectrum is flat, so the mean number of reservoir oscillators $\langle n \rangle = \langle \hat{b}_j^\dagger(0)\hat{b}_j(0) \rangle = (\exp(\hbar\omega/kT) - 1)^{-1}$ in the j th mode is independent of j . Thus the reservoir oscillators form a thermal system. The case $\langle n \rangle = 0$ corresponds to vacuum fluctuations (zero-temperature heat bath). It is convenient to consider the quantum dynamics of the system (56)–(59) in the interaction picture. Then the master equation for the density operator $\hat{\rho}$ is given by

$$\begin{aligned} \frac{\partial \hat{\rho}}{\partial \tau} = & -i \left[\frac{1}{2} \hat{a}^\dagger \hat{a}^2 + i \mathcal{F} (\hat{a}^\dagger - \hat{a}), \hat{\rho} \right] + \frac{\gamma}{2} (2\hat{a}\hat{\rho}\hat{a}^\dagger - \hat{a}^\dagger\hat{a}\hat{\rho} - \hat{\rho}\hat{a}^\dagger\hat{a}) \\ & + \gamma \langle n \rangle (\hat{a}^\dagger\hat{\rho}\hat{a} + \hat{a}\hat{\rho}\hat{a}^\dagger - \hat{a}^\dagger\hat{a}\hat{\rho} - \hat{\rho}\hat{a}\hat{a}^\dagger) \end{aligned} \quad (62)$$

where $\tau = t\chi$ is the redefined time, $\gamma = \Gamma/\chi$, and $\mathcal{F} = F/\chi$. The term $\omega\hat{a}^\dagger\hat{a}$ does not appear in Eq.(62) as a consequence of the interaction picture.

The master equation (62) can be transformed to a c -number partial differential equation. Three kinds of equations can be derived from (62): (1) an equation for the Wigner function $\Phi_{(\text{Sym})}$ related to symmetric (Weyl) ordering of the field operators \hat{a}, \hat{a}^\dagger , (2) an equation for the Wigner-like function $\Phi_{(A)}$ related to antinormal ordering of the operators, and (3) an equation for the Wigner-like function Φ_N related to normal ordering. The statistical properties of the Φ functions are discussed fully in the book by Peřina [168]. These are quasidistribution functions in the complex plane (α, α^*) , where the quantity α is

an eigenvalue of the annihilation operator \hat{a} , i.e. $\hat{a} | \alpha \rangle = \alpha | \alpha \rangle$. Here, $| \alpha \rangle$ is a coherent state.

For convenience we introduce the so-called s ordering of the field operators \hat{a}, \hat{a}^\dagger . Then we can write $\Phi_{(\text{Sym})} = \Phi_{(0)}$, $\Phi_{(A)} = \Phi_{(-1)}$ and $\Phi_{(N)} = \Phi_{(1)}$.

From (62) we get the generalized Fokker–Planck equation for the quasidistribution $\Phi_{(s)}(\alpha^*, \alpha; \tau)$ related to the s ordering [165]:

$$\frac{\partial \Phi_{(s)}}{\partial \tau} = L_{\text{class}} + L_{\text{quant}} \quad (63)$$

where

$$\begin{aligned} L_{\text{class}} &= \frac{\partial}{\partial \alpha} \left[\left(\frac{1}{2} \gamma \alpha - \mathcal{F} + i \alpha |\alpha|^2 \right) \Phi_{(s)} \right] \\ &\quad + \frac{\partial}{\partial \alpha^*} \left[\left(\frac{1}{2} \gamma \alpha^* - \mathcal{F} - i \alpha^* |\alpha|^2 \right) \Phi_{(s)} \right] + \gamma \langle n \rangle \frac{\partial^2 \Phi_{(s)}}{\partial \alpha \partial \alpha^*} \\ L_{\text{quant}} &= -i \left[(1-s) \frac{\partial}{\partial \alpha} \alpha \Phi_{(s)} - (1-s) \frac{\partial}{\partial \alpha^*} \alpha^* \Phi_{(s)} \right. \\ &\quad + \frac{s}{2} \frac{\partial^2}{\partial \alpha^2} \alpha^2 \Phi_{(s)} - \frac{s}{2} \frac{\partial^2}{\partial \alpha^{*2}} \alpha^{*2} \Phi_{(s)} \\ &\quad \left. + \frac{(s^2-1)}{4} \frac{\partial^3}{\partial \alpha^{*2} \partial \alpha} \alpha^* \Phi_{(s)} - \frac{(s^2-1)}{4} \frac{\partial^3}{\partial \alpha^2 \partial \alpha^*} \alpha \Phi_{(s)} \right] \\ &\quad + \gamma \frac{(1-s)}{2} \frac{\partial^2 \Phi_{(s)}}{\partial \alpha \partial \alpha^*} \end{aligned} \quad (64)$$

Let us emphasize that there is no difference among the equations for $\Phi_{(\text{sym})}$, $\Phi_{(A)}$, and $\Phi_{(N)}$ as long as the system (56)–(59) is classical. This problem has been studied elsewhere [176,177]. In the classical limit the term L_{quant} in Eq.(63) vanishes and $\Phi_{(s)}$ is a classical distribution function. For $L_{\text{quant}} = 0$ and $\gamma = 0$, Eq.(63) reduces to the classical Liouville equation, and for $L_{\text{quant}} = 0$ and $\gamma \neq 0$, to the classical Fokker–Planck equation. So, we can say that the L_{class} term governs classical dynamics whereas the L_{quant} term adds the quantum (operator) correction. The decision as to whether chaos appears in the system (56)–(59) can be made by investigating the separation rate of two peaks of a $\Phi_{(s)}$ function initially close to each other or by the analysis of equations for the statistical moments originating in Eq. (63). Thus, instead of attempting to solve the partial differential equation (63), we deal with the problem of solving a set of ordinary differential equations for the statistical moments.

The calculation of statistical moments with the help of $\Phi_{(s)}$ is simple. For example, if we want to calculate the average number of photons $\langle a^\dagger a \rangle$, we use one of the three function $\Phi_{(N)}$, $\Phi_{(A)}$ or $\Phi_{(\text{sym})}$. We have

$$\langle \hat{a}^\dagger \hat{a} \rangle = \int \alpha^* \alpha \Phi_{(N)}(\alpha^*, \alpha) d^2 \alpha \tag{65}$$

$$\langle \hat{a}^\dagger \hat{a} \rangle = \int (\alpha^* \alpha - 1) \Phi_{(A)}(\alpha^*, \alpha) d^2 \alpha \tag{66}$$

$$\langle \hat{a}^\dagger \hat{a} \rangle = \int \left(\alpha^* \alpha - \frac{1}{2} \right) \Phi_{(\text{sym})}(\alpha^*, \alpha) d^2 \alpha \tag{67}$$

The value of $\langle \hat{a}^\dagger \hat{a} \rangle$ is always the same, but the averaging procedure differs in each case. The relations (65)–(67) are a simple consequence of the boson commutation relation $[\hat{a}, \hat{a}^\dagger] = 1$ and the definition

$$\langle \alpha^* \alpha \rangle_{(s)} = \int \alpha^* \alpha \Phi_{(s)}(\alpha^*, \alpha) d^2 \alpha \tag{68}$$

where $\langle \alpha^* \alpha \rangle_{(N)} = \langle \hat{a}^\dagger \hat{a} \rangle$, $\langle \alpha^* \alpha \rangle_{(A)} = \langle \hat{a} \hat{a}^\dagger \rangle$, and $\langle \alpha^* \alpha \rangle_{(\text{sym})} = \frac{1}{2} \langle \hat{a}^\dagger \hat{a} + \hat{a} \hat{a}^\dagger \rangle$. It is obvious that some expectation values do not depend on ordering, for example, $\langle \hat{a}^{\dagger n} \rangle = \langle \alpha^{*n} \rangle_{(N)} = \langle \alpha^{*n} \rangle_{(A)} = \langle \alpha^{*n} \rangle_{(\text{sym})}$. The function $\Phi_{(s)}$ allows us to define the quantum cumulants. The cumulants of first order are given by

$$\langle \alpha^* \rangle_{(s)} = \xi^*, \quad \langle \alpha \rangle_{(s)} = \xi \tag{69}$$

The cumulants of second order have the forms

$$\langle \alpha^* \alpha \rangle_{(s)} - \langle \alpha^* \rangle_{(s)} \langle \alpha \rangle_{(s)} = B_{(s)} \tag{70}$$

$$\langle \alpha^{*2} \rangle_{(s)} - \langle \alpha^* \rangle_{(s)}^2 = C^* \tag{71}$$

$$\langle \alpha^2 \rangle_{(s)} - \langle \alpha \rangle_{(s)}^2 = C$$

It is easy to note that simple relations hold among $B_{(N)}$, $B_{(A)}$, and $B_{(\text{sym})}$, namely, $B_{(A)} = B_{(N)} + 1$ and $B_{(\text{sym})} = \frac{1}{2}(2B_{(N)} + 1)$. Thus the average number of photons can be expressed with the help of s ordering as follows: $\langle \hat{a}^\dagger \hat{a} \rangle = G_{(s)} + \xi^* \xi$, where $G_{(s)} = B_{(s)} - \frac{1-s}{2}$.

Analytical solutions of quantum Fokker–Planck equations such as Eq. (63) are known only in special cases. Thus, some special methods have been developed to obtain approximate solutions. One of them is the statistical moment method, based on the fact that the equation for the probability density generates an infinite hierarchic set of equations for the statistical moments and vice versa.

However, for numerical reasons the set of equations has to be truncated to a finite number, which means approximation. In this section we restrict ourselves to the second truncation (Gaussian approximation), namely, to the equations for ξ , C and $G_{(s)}$. We arrive at the following set of equations:

$$\frac{d\xi}{d\tau} = -\frac{1}{2}\gamma\xi + \mathcal{F} - i[2G_{(s)}\xi + C\xi^* + \xi^2\xi^*] \quad (72)$$

$$\frac{dC}{d\tau} = -\gamma C_{(s)} - i[\xi^2(1 + 2G_{(s)}) + C(1 + 4|\xi|^2)] - 6iG_{(s)}C \quad (73)$$

$$\frac{dG_{(s)}}{d\tau} = -\gamma G_{(s)} + i[C\xi^{*2} - C^*\xi^2] + \gamma\langle n \rangle \quad (74)$$

We examine the dynamics of this system with the initial conditions $\xi(0) = 1 + i$ and $G_{(s)}(0) = C(0) = 0$. The driving field \mathcal{F} is assumed in the form of a train of rectangular computer simulated pulses. The length of the pulse is denoted by T_1 , whereas T_2 is the distance between the pulses, and \mathcal{F}_0 is their height. Moreover, we put $\langle n \rangle = 0$, $\gamma = 0.5$, $\mathcal{F}_0 = 2$, $T_2 = 1$ and $0 < T_1 < 7.5$. The physical sense of the truncation is clear if we note that the first truncation [Eq. (63) is without s terms] gives only the classical equation for the anharmonic oscillator:

$$\frac{d\xi}{d\tau} = -\frac{1}{2}\gamma\xi + \mathcal{F}(\tau) - i\xi^2\xi^* \quad (75)$$

Thus $\langle \hat{a}^\dagger \hat{a} \rangle = |\xi|^2$ is a classical intensity. The system (75) is nonautonomous if the function \mathcal{F} is explicitly time-dependent. The autonomized version of Eq.(75) is given by

$$\begin{aligned} \frac{d\xi}{d\tau} &= -\frac{1}{2}\gamma\xi + \mathcal{F}(w) - i\xi^2\xi^* \\ \frac{dw}{d\tau} &= 1, \quad w(0) = 0 \end{aligned} \quad (76)$$

It is readily seen that the set of equations (76) consists of three equations of motion in the real variables $\text{Re}\xi$, $\text{Im}\xi$, w . If $\mathcal{F}(\tau) = \text{constant}$, chaos in the system does not appear since the set (76) becomes a two-dimensional autonomous system. The maximal Lyapunov exponents for the systems (75) and (72)–(74) plotted versus the pulse duration T_1 are presented in Fig. 36. We note that within the classical system (75) by fluently varying the length of the pulse T_1 , we turn order into chaos and chaos into order. For $0 < T_1 < 0.84$ and $1.08 < T_1 < 7.5$, the maximal Lyapunov exponents λ_1 are negative or equal to zero and, consequently, lead to limit cycles and quasiperiodic orbits. In the points where $\lambda_1 = 0$, the system switches its periodicity. The situation changes dramatically if,

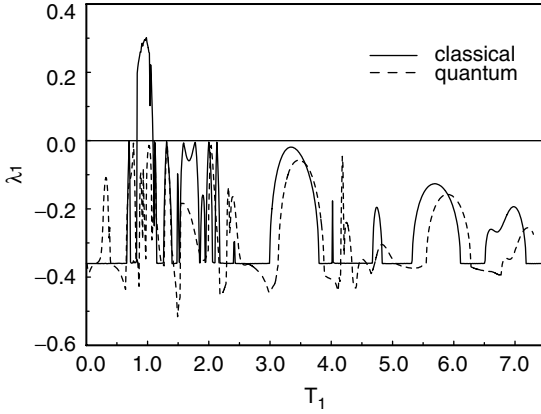


Figure 36. Maximal Lyapunov exponents for the system before (solid line) and after quantum correction (dashed line).

instead of Eq. (75), its quantum version, Eqs. (72)–(74), is taken into account. For the quantum system the maximal Lyapunov exponent is not positive, Therefore the chaotic oscillations due to quantum correction vanish (Fig. 37). The regular oscillations remain regular, but their structures change [165].

B. Chaos in Second-Harmonic Generation of Light

Let us consider a quantum optical system with two interacting modes at the frequencies ω_1 and $\omega_2 = 2\omega_1$, respectively, interacting by way of a nonlinear crystal with second-order susceptibility. Moreover, let us assume that the nonlinear crystal is placed within a Fabry–Pérot interferometer. Both modes are damped via a reservoir. The fundamental mode is driven by an external field with the frequency ω_L and amplitude F . The Hamiltonian for our system is given by [169,178]:

$$\hat{H} = \hat{H}_{\text{rev}} + \hat{H}_{\text{irrev}} \tag{77}$$

$$\begin{aligned} \hat{H}_{\text{rev}} = & \hbar\omega_1 \hat{a}_1^\dagger \hat{a}_1 + \hbar\omega_2 \hat{a}_2^\dagger \hat{a}_2 + i\hbar F (\hat{a}_1^\dagger e^{-i\omega_L t} - \hat{a}_1 e^{i\omega_L t}) \\ & + i\hbar \frac{\kappa}{2} (\hat{a}_1^{\dagger 2} \hat{a}_2 - \hat{a}_1^2 \hat{a}_2^\dagger) \end{aligned} \tag{78}$$

$$\hat{H}_{\text{irrev}} = \hbar \sum_j \sum_{i=1}^2 (\Omega_j^{(i)} \hat{b}_j^{\dagger(i)} \hat{b}_j^{(i)} + K_j^{(i)} \hat{b}_j^{(i)} \hat{a}_i^\dagger + K_j^{*(i)} \hat{b}_j^{\dagger(i)} \hat{a}_i) \tag{79}$$

where \hat{H}_{rev} describes the reversible part of interaction and \hat{H}_{irrev} is the irreversible part responsible for the loss mechanism. The quantities $\hat{a}_1, (\hat{a}_1^\dagger); \hat{a}_2, (\hat{a}_2^\dagger)$ are the

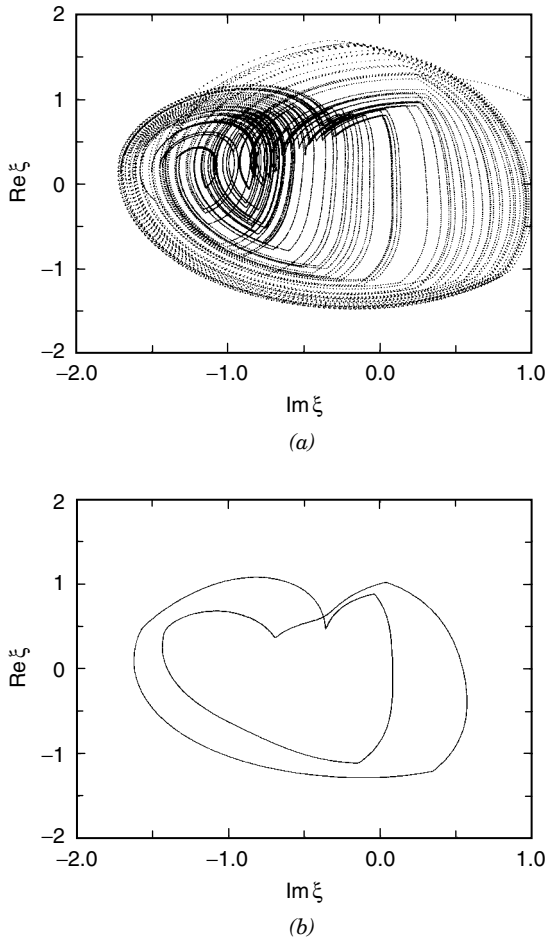


Figure 37. Phase portraits $\text{Re } \xi$ versus $\text{Im } \xi$. (a) the classical case; Eq. (75) with the initial condition $\xi(0) = 1 + i$. The parameters of the pulse are $T_1 = 0.98, T_2 = 1$, and $F_0 = 2$. The damping constant is $\gamma = 0.5$, and the time is $100 < \tau < 200$. (b) The quantum system; Eqs. (72)–(74) with the initial conditions $\xi(0) = 1 + i$ and $G_{(s)}(0) = C(0) = 0$. The parameters of the pulse are $T_1 = 0.98, T_2 = 1$, and $F_0 = 2$. The damping constant is $\gamma = 0.5$, and the time $100 < \tau < 200$.

photon annihilation (creation) operators for the fundamental and second-harmonic modes, respectively. The parameter κ is taken to be real and acts as a nonlinear coupling constant between the two modes. Finally, the operators $\hat{b}_j^{\dagger(i)}, \hat{b}_j^{(i)}$ are the boson annihilation (creation) operators of the reservoir. The frequencies of the reservoir oscillations are denoted by $\Omega_j^{(i)}$ and the coupling constant between the optical and reservoir modes, by $K_j^{(i)}$. The dynamics of the

system (77) on eliminating the reservoir Hamiltonian (79) is governed by the appropriate master equation for the density operator $\hat{\rho}$. The master equation in the interaction picture leads to the following c -number Fokker–Planck equation for the quasidistribution function $\Phi_{(s)}$ [168,169,178]

$$\frac{\partial \Phi_{(s)}}{\partial \tau} = L_{\text{class}} + L_{\text{quant}} \quad (80)$$

where

$$L_{\text{class}} = \sum_{i=1}^2 \left[\gamma_i \frac{\partial}{\partial \alpha_i} (\alpha_i \Phi_{(s)}) + \gamma_i \frac{\partial}{\partial \alpha_i^*} (\alpha_i^* \Phi_{(s)}) + \frac{\partial}{\partial \alpha_i} (D_i \Phi_{(s)}) + \frac{\partial}{\partial \alpha_i^*} (D_i^* \Phi_{(s)}) + \gamma_i \langle n_i \rangle \frac{\partial^2 \Phi_{(s)}}{\partial \alpha_i^* \partial \alpha_i} \right] \quad (81)$$

$$L_{\text{quant}} = \left(\frac{1-s}{2} \right) \sum_{i=1}^2 \gamma_i \frac{\partial^2 \Phi_{(s)}}{\partial \alpha_i^* \partial \alpha_i} - \frac{s}{2} \frac{\partial^2}{\partial \alpha_1^2} (D_{11} \Phi_{(s)}) - \frac{s}{2} \frac{\partial^2}{\partial \alpha_1^{*2}} (D_{11}^* \Phi_{(s)}) \quad (82)$$

The quasidistribution function $\Phi_{(s)}$ is defined as follows: $\Phi_{(s=1)} = P$ and $\Phi_{(s=-1)} = Q$. The function $\Phi_{(s)}$ is determined in the complex plane $(\alpha_1, \alpha_2, \alpha_1^*, \alpha_2^*)$, where α_i is an eigenvalue of the annihilation operator \hat{a}_i , namely, $\hat{a}_i |\alpha_i\rangle = \alpha_i |\alpha_i\rangle$. Here, $|\alpha_i\rangle$ is a coherent state. The initial condition for the Fokker–Planck equation is given by

$$\Phi_{(s)}(\alpha_1(\tau), \alpha_2(\tau); \tau)|_{\tau=0} = \Phi_{(s)}(\alpha_1(0) = \alpha_{10}, \alpha_2(0) = 0; 0) \quad (83)$$

which means that the amplitude of the fundamental mode initially differs from zero whereas the amplitude of the second harmonic equals zero. The coefficients D_i and D_{11} are given by

$$\begin{aligned} D_1 &= -\mathcal{F} - \alpha_1^* \alpha_2 \\ D_1^* &= -\mathcal{F} - \alpha_1 \alpha_2^* \\ D_2 &= 0.5 \alpha_1^2 \\ D_2^* &= 0.5 \alpha_1^{*2} \\ D_{11} &= \frac{\partial D_1}{\partial \alpha_1^*} = -\alpha_2 \\ D_{11}^* &= \frac{\partial D_1^*}{\partial \alpha_1} = -\alpha_2^* \end{aligned} \quad (84)$$

The general relations among the coefficients D_i and D_{ij} are presented elsewhere [179]. The quantities γ_1 and γ_2 are the damping constants for the fundamental and second-harmonic modes, respectively. In Eq.(82) we shall restrict ourselves to the case of zero-frequency mismatch between the cavity and the external forces ($\omega_1 - \omega_L = 0$). In this way we exclude the rapidly oscillating terms. Moreover, the time τ and the external amplitude \mathcal{F} have been redefined as follows: $\tau = \kappa t$ and $\mathcal{F} = \frac{F}{\kappa}$. The s ordering in Eq.(80) which is responsible for the operator structure of the Hamiltonian allows us to contrast the classical and quantum dynamics of our system. If the Hamiltonian (77)–(79) is classical (i.e., if it is a c number), then the equation for the probability density has the form of Eq.(80) without the s terms:

$$-\frac{s}{2} \frac{\partial^2}{\partial \alpha_1^2} (D_{11} \Phi_{(s)}) - \frac{s}{2} \frac{\partial^2}{\partial \alpha_1^{*2}} (D_{11}^* \Phi_{(s)}), \quad \gamma_i \left(\frac{1-s}{2} \right) \frac{\partial^2 \Phi_{(s)}}{\partial \alpha_i^* \partial \alpha_i}$$

The s terms distinguish the classical and quantum dynamics quite naturally. If they do not appear, the difference between P and Q vanishes.

The Fokker–Planck equation (80) generates an infinite and hierarchic set of equations for the statistical moments (see Section IV.A.1). Below, we restrict ourselves to a Gaussian approximation. The cumulants are defined by the following relations:

$$\xi_i = \langle \hat{a}_i \rangle \quad (85)$$

$$B_i = \langle \hat{a}_i^\dagger \hat{a}_i \rangle - \langle \hat{a}_i^\dagger \rangle \langle \hat{a}_i \rangle \quad (86)$$

$$B_{12} = \langle \hat{a}_1^\dagger \hat{a}_2 \rangle - \langle \hat{a}_1^\dagger \rangle \langle \hat{a}_2 \rangle \quad (87)$$

$$C_i = \langle \hat{a}_i^2 \rangle - \langle \hat{a}_i \rangle^2 \quad (88)$$

$$C_{12} = \langle \hat{a}_1 \hat{a}_2 \rangle - \langle \hat{a}_1 \rangle \langle \hat{a}_2 \rangle \quad (89)$$

Integration per partes of the Fokker–Planck equation for the quasidistribution $\Phi_{(s=1)} = P$ (the choice of a particular s is a question of taste only) allows us to write the appropriate equations for the cumulants. In what follows, we assume that damping is included only by way of coupling to the reservoir at zero temperature, that is, $\langle n_i \rangle = 0$. The first truncation (the cumulants higher than first-order vanish) leads to the classical limit. Then, from Eq. (80), we get the classical Bloembergen equations [102] [see Eqs. (1)]:

$$\frac{d\xi_1}{dt} = -\gamma_1 \xi_1 + \mathcal{F} + \xi_1^* \xi_2 \quad (90)$$

$$\frac{d\xi_2}{dt} = -\gamma_2 \xi_2 - 0.5 \xi_1^2 \quad (91)$$

The initial conditions have the following form:

$$\xi_1(0) = \xi_{10}, \quad \xi_2(0) = 0 \quad (92)$$

The s terms in Eq. (80) contribute nothing to the preceding equations. The second-order truncation (Gaussian approximation) leads to the following set of equations:

$$\frac{d\xi_1}{d\tau} = -\gamma_1\xi_1 + \mathcal{F} + \xi_1^*\xi_2 + B_{12} \quad (93)$$

$$\frac{d\xi_2}{d\tau} = -\gamma_2\xi_2 - 0.5(\xi_1^2 + C_1) \quad (94)$$

$$\frac{dB_1}{d\tau} = -2\gamma_1B_1 + B_{12}^*\xi_1 + B_{12}\xi_1^* + C_1^*\xi_2 + C_1\xi_2^* \quad (95)$$

$$\frac{dB_2}{d\tau} = -2\gamma_2B_2 - B_{12}^*\xi_1 - B_{12}\xi_1^* \quad (96)$$

$$\frac{dC_1}{d\tau} = -2\gamma_1C_1 + 2(C_{12}\xi_1^* + B_1\xi_2) + \xi_2 \quad (97)$$

$$\frac{dC_2}{d\tau} = -2\gamma_2C_2 - 2C_{12}\xi_1 \quad (98)$$

$$\frac{dC_{12}}{d\tau} = -(\gamma_1 + \gamma_2)C_{12} + B_{12}\xi_2 - C_1\xi_1 + C_2\xi_1^* \quad (99)$$

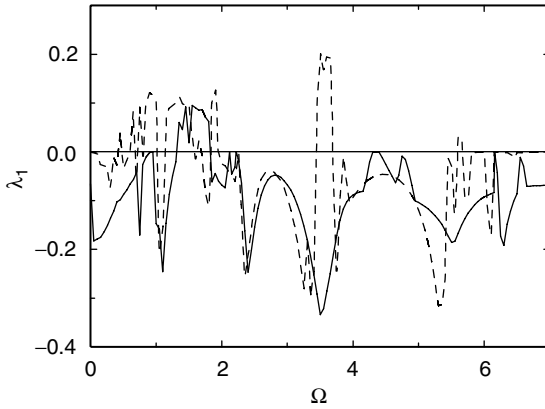
$$\frac{dB_{12}}{d\tau} = -(\gamma_1 + \gamma_2)B_{12} + C_{12}\xi_2^* + \xi_1(B_2 - B_1) \quad (100)$$

The set of equations (93)–(100), proposed for the first time by Peřina et al. [169], is a development of the Bloembergen equations (90)–(91). The initial conditions with respect to (83) are given by

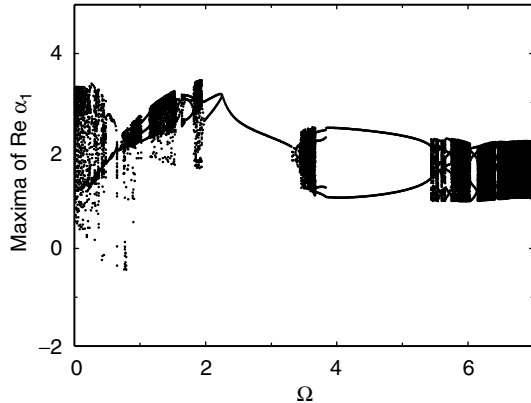
$$\begin{aligned} \xi_1(0) &= \xi_{10}, & \xi_2(0) &= \xi_{20} = 0 \\ B_{1,2}(0) &= B_{12}(0) = C_{1,2}(0) = C_{12}(0) = 0 \end{aligned} \quad (101)$$

The s terms in Eq. (80) contribute only the term ξ_2 in Eq. (97). Thus, the term ξ_2 represents the quantum diffusional s -terms in the Fokker–Planck equation. The other terms in Eqs. (93)–(100) originate in the drift terms of the Fokker–Planck equation. The terms B_{12} and C_1 in Eqs. (93)–(94) play the role of feedback terms that pump quantum fluctuations into the classical Bloembergen equations. If the s terms in Eq. (80) do not appear (the classical case), the term ξ_2 in Eq. (97) does not appear, either. In this case the subset (95)–(100) with zero initial conditions has zero solutions and in consequence leads to the first truncation [171].

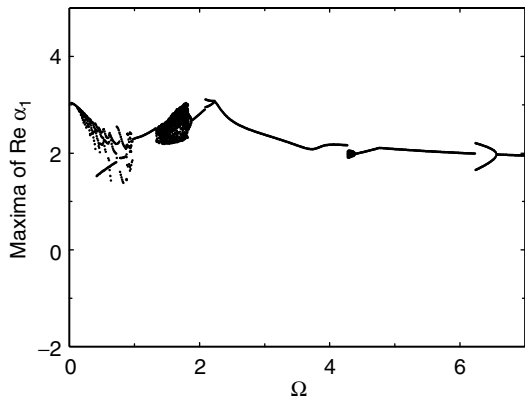
Let us consider the driving field amplitude in the form $\mathcal{F} = \mathcal{F}_0(1 + \sin \Omega\tau)$, meaning that the external pump amplitude is modulated with a frequency Ω



(a)



(b)



(c)

Figure 38. The classical (dashed) and quantum (solid line) maximal Lyapunov exponents (a) and the appropriate bifurcation maps (b,c) versus the modulated parameter Ω . The parameters are

around \mathcal{F}_0 . For the time-independent field $\mathcal{F} = \mathcal{F}_0$ ($\Omega = 0$), the system does not manifest chaotic behavior. However, a change of Ω in the range $0 < \Omega < 7$ leads the system from periodic to chaotic motion or vice versa. The dynamical behavior of our system is reflected by the Lyapunov exponents. The maximal Lyapunov exponents as a function of the modulation parameter Ω for the classical case [Eqs. (90)–(91)] (dashed line) and for the quantum case [Eqs. (93)–(100)] (solid line) is plotted in Fig. 38a. For the classical case, one observes several regions where the system behaves chaotically ($\lambda_1 > 0$) whereas elsewhere it behaves orderly ($\lambda_1 < 0$). For the quantum case we observe only one region of chaos $1.3 < \Omega < 1.72$, which does not overlap exactly any classical region of chaos. Generally, as is seen in Fig. 38, the quantum correction reduces chaos in the system but does not eliminate it completely. For example, for $\Omega = 1.4$, both the classical and quantum versions of the system behave chaotically whereas the classical maximal Lyapunov exponent is greater than quantum. This means a reduction of chaos in the classical system due to the quantum correction. The reduction is also reflected by the appropriate bifurcation diagrams (Fig. 38b,c). Another useful way to visualize the reduction of chaos is to analyze the motion in the phase space. However, in our case, the classical phase space is four-dimensional ($\text{Re}\xi_1, \text{Im}\xi_1, \text{Re}\xi_2, \text{Im}\xi_2$). This means that we can compare only the motion in the reduced phase space. For physical interpretation it is convenient to consider the motion in two-dimensional intensity space ($I_1 = |\xi_1|^2, I_2 = |\xi_2|^2$). Then, instead of a typical *phase portrait*, we deal with an *intensity portrait*. In the quantum case the intensities are the average numbers of photons determined by $\langle \hat{a}_i^\dagger \hat{a}_i \rangle = |\xi_i|^2 + B_i$, where B_i is the quantum correction to the classical intensity $I_i = |\xi_i|^2$.

The reduction of chaos for $\Omega = 1.45$ is presented in the intensity portraits of Fig. 39. However, as is seen in Fig. 38a, there is a small region ($1.68 < \Omega < 1.80$) where the system behaves orderly in the classical case but the quantum correction leads to chaos. By way of an example for $\Omega = 1.75$, the classical system, after quantum correction, loses its orderly features and the limit cycle settles into a chaotic trajectory. Generally, Lyapunov analysis shows that the transition from classical chaos to quantum order is very common. For example, this kind of transition appears for $\Omega = 3.5$ where chaos is reduced to periodic motion on a limit cycle. Therefore a global reduction of chaos can be said to take place in the whole region of the parameter $0 < \Omega < 7$.

As we see in Fig. 38, transitions leading from classical order to quantum order are also possible. For example, for $\Omega = 6.7$ the quasiperiodic classical motion is reduced to periodic motion after the quantum correction.

C. Final Remarks

Using a cumulant expansion, we have shown how to obtain *quantum corrections* to purely classical equations of motion. Quantum correction reduces chaos in

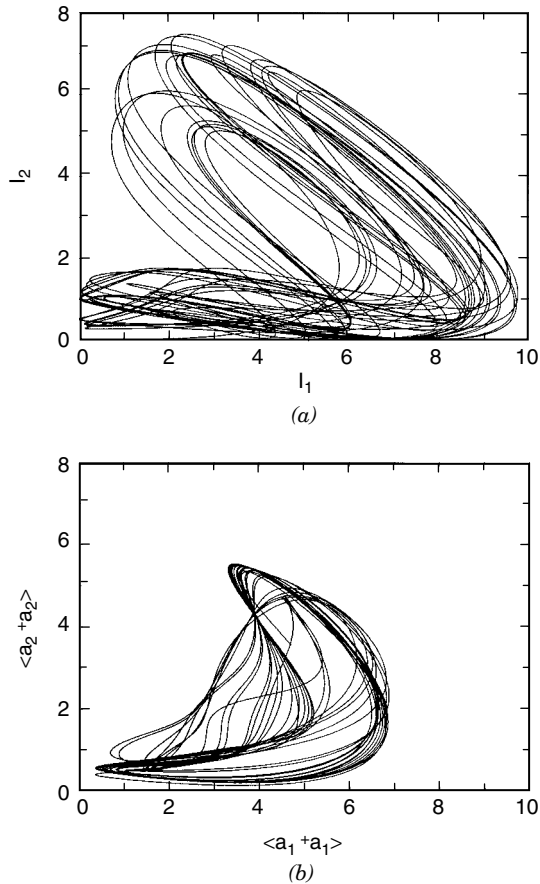


Figure 39. Transition from classical chaos (a) to quantum chaos (b). The parameters are those of Fig. 38 but with $\Omega = 1.4$.

the classical systems. The Lyapunov analysis and bifurcation maps show that after the first quantum correction, the number of chaotic regions is reduced, although not eliminated fully. The question is what happens if third-order or higher-order corrections are taken into account?. Let us note that, for example, the set (72)–(74) consists of 5 equations in real variables. If third-order truncation is performed, the set (72)–(74) is additionally modified and supplemented with four equations in real variables, thus leading to 9 equations. The fourth truncation leads to 15 equations in real variables, and so on. From the formal point of view, the quantum corrections become more and more rigorous with higher and higher order of the approximation. On the other hand, even if

the numerical calculations are performed in extended precision, computer errors can accumulate significantly, leading to spurious high-order quantum corrections due to the increasing numbers of equations and iterations. The quantum Lyapunov whose classical counterpart is positive has to be calculated with a finite time, empirically expressed. The time is of the rank $(\lambda)^{-1}$, where λ is the classical Lyapunov exponent [158].

References

1. H. Poincaré, *Les methodes nouvelle de la mécanique céleste*, Gauthier-Villars, 1892.
2. E. N. Lorenz, *J. Atmos. Sci.* **20**, 130 (1963).
3. P. Cvitanović, *Universality in Chaos*, Adam Hilger Ltd, Bristol, UK, 1984.
4. G. Casati (ed), *Chaotic Behaviour in Quantum Systems*, Plenum Press, New York, 1985.
5. H. G. Schuster, *Deterministic Chaos. An Introduction*, VCH Verlagsgesellschaft, Weinheim, 1988.
6. M. C. Gutzwiller, *Chaos in Classical and Quantum Systems*, Springer-Verlag, New York, 1990.
7. E. Ott, *Chaos in Dynamical Systems*, Cambridge Univ. Press, New York, 1993.
8. R. C. Hilborn, *Chaos and Nonlinear Dynamics*, Oxford Univ. Press, New York, 1994.
9. Special Issue, *Instabilities in Active Optical Media*, *J. Opt. Soc. Am. B* **2**(1) (1985).
10. Special Issue, *Spatio-temporal Coherence and Chaos in Physical Sytems*, *Physica D* **23** (1986).
11. R. W. Boyd, M.G. Raymer, and L.M. Narducci (Eds.), *Optical Instabilities*, Cambridge Univ. Press, London, 1986.
12. F. T. Arecchi and R. G. Harrison, *Instabilities and Chaos in Quantum Optics*, in *Springer Series in Synergetics*, Vol. 34, Springer-Verlag, Berlin, 1987.
13. P. W. Milonni, M.L. Shih, and J.R. Ackerhalt, *Chaos in Laser-Matter Interactions*, World Scientific, Singapore, 1987.
14. L. W. Caspersen, *Spontaneous pulsations in Lasers*, in J. D. Harvey and D. F. Walls (Eds.), *Laser Physics, Lecture Notes in Physics*, Vol. 182, Springer-Verlag, Berlin, 1983.
15. E.R. Buley and F.W. Cummings, *Phys. Rev.* **134**, A1454 (1964).
16. H. Haken, *Phys. Lett. A* **53**, 77 (1975).
17. R. Graham, *Phys. Lett. A* **58**, 440 (1976).
18. F. Yamada and R. Graham, *Phys. Rev. Lett.* **45**, 1322 (1980).
19. M.-L. Shih and P.W. Milloni, *Opt. Commun.* **49**, 155 (1984).
20. H. Zeghlache and P. Mandel, *J. Opt. Soc. Am. B* **2**,18 (1985).
21. T. Ogawa, *Phys. Rev. A* **37**, 4286 (1988).
22. R. G. Harrison and D. J. Biswas, *Prog. Quantum Electron.* **10**, 147 (1985).
23. P. W. Milonni, J. R. Ackerhalt, and M.-L. Shih, *Opt. Commun.* **49**, 155 (1984).
24. M.-L. Shih, P.W. Milonni, and J. R. Ackerhalt, *J. Opt. Soc. Am. B* **2**, 130 (1985).
25. L. W. Caspersen and A. Yariv, *Appl. Phys. Lett.* **17**, 259 (1970).
26. L. W. Caspersen, *Phys. Rev. A* **21**, 911 (1980).
27. M. Mayr, H. Risken, and H.D. Vollmer,, *Opt. Commun.*, **36**, 480 (1981).
28. P. Mandel, *Opt. Commun.* **44**, 400 (1983).
29. D. K. Bandy, L. M. Narducci, L.A. Lugiato, and N.B. Abraham, *J. Opt. Soc. Am. B* **2**, 56 (1985).

30. F. T. Arecchi, R. Meucci, G. Puccioni, and J. Tredicce, *Phys. Rev. Lett.* **49**, 1217 (1982).
31. L. W. Casperson, *IEEE J. Quantum Electron.* **QE-14**, 756 (1978).
32. C. O. Weiss and H. King, *Opt. Commun.* **44**, 59 (1982).
33. R. S. Gioggia and N.B. Abraham, *Phys. Rev. Lett.* **51**, 650 (1983).
34. L. M. Hoffer, T.H. Chyba, and N. B. Abraham, *J. Opt. Soc. Am. B* **2**, 102 (1985).
35. N. B. Abraham, T. Chyba, M. Coleman, R. S. Gioggia, N. J. Halas, L. M. Hoffer, S.-N. Liu, M. Maeda, and J.C. Wesson, in J. D. Harvey and D.F. Walls (Eds.), *Laser Physics, Lecture Notes in Physics* Vol. 182, Springer-Verlag, Berlin, 1983.
36. C. O. Weiss and W. Klische, *Opt. Commun.* **51**, 47 (1984).
37. C. O. Weiss, W. Klische, P.S. Ering, and M. Cooper, *Opt. Commun.* **52**, 405 (1985).
38. C. O. Weiss and J. Brock, *Phys. Rev. Lett.* **57**, 2804 (1986).
39. C. O. Weiss, N. B. Abraham, and V. H. Hübner, *Phys. Rev. Lett.* **61**, 1587 (1988).
40. D. J. Biswas and R.G. Harrison, *Phys. Rev. A* **32**, 3835 (1985).
41. T. Midavaine, D. Dangoisse, and P. Glorieux, *Phys. Rev. Lett.* **55**, 1989 (1985).
42. F. Hollinger and C. Jung, *J. Opt. Soc. Am. B* **2**, 218 (1985).
43. W. Klische, H. R. Telle, and C. O. Weiss, *Opt. Lett.* **9**, 561 (1984).
44. Y. C. Chen, H. G. Winful, and J. M. Liu, *Appl. Phys. Lett.* **47**, 208 (1985).
45. H. G. Winful, Y. C. Chen, and J. M. Liu, *Appl. Phys. Lett.* **48**, 616 (1986).
46. T. Baer, *J. Opt. Soc. Am. B* **3**, 1175 (1986).
47. C. Barcikowski and R. Roy, *Phys. Rev. A* **43**, 6455 (1991).
48. C. Barcikowski, R. F. Fox, and R. Roy, *Phys. Rev. A* **45**, 403 (1992).
49. J. Ye, H. Li, and J. G. McInerney, *Phys. Rev. A* **47**, 2249 (1993).
50. E. Ott, C. Grebogi, and J. A. Yorke, *Phys. Rev. Lett.* **64**, 1196 (1990).
51. R. Roy, T.W. Murphy, Jr., T. D. Maier, Z. Gills, and E. R. Hunt, *Phys. Rev. Lett.* **68**, 1259 (1992).
52. K. Pyragas, *Phys. Lett. A* **170**, 421 (1992).
53. S. Bielawski, D. Derozier, and P. Glorieux, *Phys. Rev. E* **49**, R971 (1994).
54. R. Meucci, M. Ciofini, and R. Labate, *Phys. Rev. E* **53**, R5537 (1996).
55. R. Meucci, R. Labate, and M. Ciofini, *Phys. Rev. E* **56**, 2829 (1997).
56. P. Glorieux, *Int. J. Bifurcation Chaos* **8**, 1749 (1998).
57. R. Roy, and K. S. Thornburg, *Phys. Rev. Lett.* **72**, 2009 (1994).
58. P. Colet and R. Roy, *Opt. Lett.* **19**, 2056 (1994).
59. P. M. Alsing, A. Gavrielidies, V. Kovanis, R. Roy, and K. S. Thornburg, *Phys. Rev. E* **56**, 6302 (1997).
60. G. D. Van Wiggeren and R. Roy, *Phys. Rev. Lett.* **81**, 3547 (1998).
61. S. Bocattelli, C. Grebogi, Y.-C. Lai, H. Mancini, and D. Maza, *Phys. Rep.* **329**, 103 (2000).
62. P. I. Bielobrov, G. M Zaslavski, and G.T. Tartakovski, *JETP* **44**, 945 (1977).
63. P. W. Milonni, J. R. Ackerhalt, and H. W. Galbraith, *Phys. Rev. Lett.* **50**, 966 (1983).
64. M. Munz, *Z. Phys. B* **53**, 311 (1983).
65. M. Kuś, *Phys. Rev. Lett.* **54**, 1343 (1985).
66. R. F. Fox and J. Edison, *Phys. Rev. A* **34**, 482 (1986).
67. J. Edison and R. F. Fox, *Phys. Rev. A* **34**, 3288 (1986).
68. A. Nath and D. S. Ray, *Phys. Rev. A* **36**, 431 (1987).

69. C. Boden, M. Dämmig, and F. Mitschke, *Phys. Rev. A* **45**, 6829 (1992).
70. K. Ikeda, *Opt. Commun.* **30**, 257 (1979).
71. K. Ikeda, H. Daido, and O. Akimoto, *Phys. Rev. Lett.* **45**, 709 (1980).
72. L. A. Lugiato, *Opt. Commun.* **33**, 108 (1980).
73. H. J. Carmichael, R. R. Snapp, and W. C. Schieve, *Phys. Rev. A* **26**, 3408 (1982).
74. R. R. Snapp, H. J. Carmichael, and W. C. Schieve, *Opt. Commun.* **40**, 68 (1981).
75. H. M. Gibbs, F. A. Hopf, D. L. Kaplan, and R. L. Shoemaker, *Phys. Rev. Lett.* **46**, 474 (1981).
76. H. Nakatsuka, S. Asaka, H. Itoh, K. Ikeda, and M. Matsuoka, *Phys. Rev. Lett.* **50**, 109 (1983).
77. F. A. Hopf, D. L. Kaplan, H. M. Gibbs, and R. L. Shoemaker, *Phys. Rev. A* **25**, 2172 (1982).
78. K. Ikeda and O. Akimoto, *Phys. Rev. Lett.* **48**, 617 (1982).
79. L. A. Lugiato, L. M. Narducci, D. K. Brandy, and C. A. Pennise, *Opt. Commun.* **43**, 281 (1982).
80. C. M. Savage, H. J. Carmichael, and D. F. Walls, *Opt. Commun.* **42**, 211 (1982).
81. H. J. Carmichael, C. M. Savage, and D. F. Walls, *Phys. Rev. Lett.* **50**, 163 (1983).
82. C. Parigger, P. Zoller, and D. F. Walls, *Opt. Commun.* **44**, 213 (1983).
83. C. M. Savage, and D. F. Walls, *Optica Acta* **30**, 557 (1983).
84. G. J. Milburn, *Phys. Rev. A* **41**, 6567 (1990).
85. J. R. Ackerhalt, H. W. Galbraith, and P.W. Milonni, *Phys. Rev. Lett.* **51**, 1259 (1983).
86. J. R. Ackerhalt and P. W. Milonni, *Phys. Rev. A* **34**, 1211 (1986).
87. J. R. Ackerhalt and P. W. Milonni, *Phys. Rev. A* **37**, 1552 (1987).
88. H. W. Galbraith, J. R. Ackerhalt, and P.W. Milonni, *J. Chem. Phys.* **79**, 5345 (1983).
89. P. W. Milonni, J. R. Ackerhalt, and H. W. Golbraith, *Phys. Rev. A* **28**, 887 (1983).
90. A. Nath and D. S. Ray, *Phys. Rev. A* **35**, 1959 (1987).
91. C. J. Candall and J. R. Albritton, *Phys. Rev. Lett.* **52**, 1887 (1984).
92. W. Lu and R. G. Harrison, *Europhys. Lett.* **16**, 655 (1991).
93. J. M. Wesinger, J. M. Finn, and E. Ott, *Phys. Rev. Lett.* **44**, 453 (1980).
94. D. S. Ray, *Phys. Rev. A* **29**, 3440 (1984).
95. W. Krolikowski, M. R. Belic, M Cronin-Golomb, and A. Bledowski, *J. Opt. Soc. Am.* **B7**, 1204 (1990).
- 96/97. S. Wabnitz, *Phys. Rev. Lett.* **58**, 1415 (1987).
98. P. A. Franken, A. E. Hill, C. W. Peters, and G. Weinreich, *Phys. Rev. Lett.* **7**, 118 (1961).
99. J. A. Armstrong, N. Bloembergen, J. Ducuing, and P. S. Pershan, *Phys. Rev.* **127**, 1918 (1962).
100. D. S. Chemla, *Rep. Prog. Phys.* **43**, 1191 (1980).
101. S. Kielich, *Molecular Nonlinear Optics*, Nauka, Moscow, 1986 (in Russian).
102. N. Bloembergen, *Nonlinear Optics*, Benjamin, New York, 1965.
103. R. Tanas, "Quantum noise in nonlinear optical phenomena," first chapter in Part 1 of this three-volume set.
104. P. D. Drummond, K. J. McNeil and D. F. Walls, *Optica Acta* **27**, 321 (1980).
105. P. Mandel and T. Erneux, *Optica Acta* **29**, 7 (1982).
106. L. A. Lugiato, C. Oldano, C. Fabre, E. Giacobino, and R. J. Horowicz, *Nuovo Cim. D* **10**, 959 (1988).
107. K. Grygiel and P. Szlachetka, *Opt. Commun.* **78**, 177 (1990).
108. K. Grygiel and P. Szlachetka, *Opt. Commun.* **91**, 241 (1992).

109. N. V. Alekseeva, K. N. Alekseev, G. P. Berman, A. K. Popov, and V. Z. Yakhnin, *Quantum Opt.* **3**, 323 (1991).
110. K. Grygiel and P. Szlachetka, *Opt. Commun.* **158**, 112 (1998).
111. K. Grygiel, manuscript in preparation.
112. G. Benettin, L. Galgani, and J.-M. Strelcyn, *Phys. Rev. A* **14**, 2338 (1976).
113. J. P. Eckmann and D. Ruelle, *Rev. Mod. Phys.* **57**, 617 (1985).
114. A. Wolf, J. B. Swift, H. L. Swinney, and J. A. Vastano, *Physica* **D16**, 285 (1985).
115. K. Grygiel and P. Szlachetka, *Acta Phys. Polon. B* **26**, 1321 (1995).
116. O. E. Roessler, *Phys. Lett. A* **71**, 155 (1979).
117. T. Kapitaniak and W.-H. Steeb, *Phys. Lett. A* **152**, 33 (1991).
118. S. P. Dawson, *Phys. Rev. Lett.* **76**, 4348 (1996).
119. E. Barreto, B. H. Hunt, C. Grebogi, and J.A. York, *Phys. Rev. Lett.* **78**, 4561 (1997).
120. K. Stefański, *Chaos Solit. Fract.* **9**, 83 (1998).
121. M. A. Harrison and Y.-C. Lai, *Phys. Rev. E* **59**, R3799 (1999).
122. L. Yang, Z. Liu, and J. Mao, *Phys. Rev. Lett.* **84**, 67 (2000).
123. P. Szlachetka and K. Grygiel, in W. Florek, D. Lipiński, and T. Lulek, (Eds.), *Symmetry and Structural Properties of Condensed Matter*, 2nd Int. School of Theoretical Physics (Poznań, 1992), World Scientific, Singapore, 1993, pp. 221–236.
124. S. Hayes, C. Grebogi, E. Ott, and A. Mark, *Phys. Rev. Lett.* **73**, 1781 (1994).
125. L. M. Pecora and T. L. Carroll, *Phys. Rev. Lett.* **64**, 821 (1990).
126. L. M. Pecora and T. L. Carroll, *Phys. Rev. A* **44**, 2374 (1991).
127. T. Kapitaniak, *Phys. Rev. E* **50**, 1642 (1994).
128. S. P. Raj, S. Rajasekar, and K. Murali, *Phys. Lett. A* **264**, 283 (1999).
129. N. Platt, E. A. Spiegel, and C. Tresser, *Phys. Rev. Lett.* **70**, 279 (1993).
130. Y. C. Lai and C. Grebogi, *Phys. Rev. E* **52**, R3313 (1995).
131. H. Sun, S. K. Scott, and K. Showalter, *Phys. Rev. E* **60**, 3876 (1999).
132. F. Heagy, T. L. Carroll, and L. M. Pecora, *Phys. Rev. Lett.* **73**, 3528 (1994).
133. J. H. Eberly, N. B. Narozhny, and J. J. Sanchez-Mondragon, *Phys. Rev. Lett.* **44**, 1323 (1980).
134. B. W. Shore and P.L. Knight, *J. Mod. Opt.* **40**, 1195 (1993).
135. M. Kozierowski and S. M. Chumakov, *Phys. Rev. A* **52**, 4194 (1995).
136. S. M. Jensen, *IEEE J. Quantum Electron.* **QE-18**, 1580 (1982).
137. V. M. Kenkre and D.K. Campbell, *Phys. Rev. B* **34**, 4959 (1986).
138. A. Cheffles and S.M. Barnett, *J. Mod. Opt.* **43**, 709 (1996).
139. J. Fiurášek, J. Křepelka, and J. Peřina, *Opt. Commun.* **167**, 115 (1999).
140. V. Peřinová and M. Karská, *Phys. Rev. A* **39**, 4056 (1989).
141. E. T. Whittaker, *A Treatise on the Analytical Dynamics of Particles and Rigid Bodies with an Introduction to the Problem of Three Bodies*, Cambridge Univ. Press, Cambridge, UK, 1952.
142. K. Grygiel and P. Szlachetka, *Opt. Commun.* **177**, 425 (2000).
143. N. Minorsky, *Nonlinear Oscillations*, Van Nostrand, Princeton, NJ, 1962, p. 285.
144. L. Gammaitoni, F. Marchesoni, and S. Santucci, *Phys. Lett. A* **195**, 116 (1994).
145. L. Gammaitoni, P. Hänggi, P. Jung, and F. Marchesoni, *Rev. Mod. Phys.* **70**, 223 (1998).
146. N. Korolkowa and J. Peřina, *Opt. Commun.* **136**, 135 (1996).

147. S. R. Friberg, A. M. Weiner, Y. Silberberg, B. G. Sfez, and P. S. Smith, *Opt. Lett.* **13**, 904 (1998).
148. Lj. Kocarev, K. Halle, K. Eckert, and L. O. Chua, *Int. J. Bifurc. Chaos* **2**, 706 (1992).
149. K. M. Cuomo and A.V. Oppenheim, *Phys. Rev. Lett.* **71**, 65 (1993).
150. P. D. Townsend, G. L. Baker, J. L. Jackel, J. A. Shelburne III, and S. Etemand, SPIE Vol. 1147, *Nonlinear Properties of Organic Materials II*, 1989, p. 256.
151. G. Casati, B. Chirikov, J. Ford, and F.M. Izrailev, in G. Casati and J. Ford, (Eds.), *Stochastic Behavior in Classical and Quantum Hamiltonian Systems of Lecture Notes in Physics*, Vol. 93, Springer, Berlin, 1979.
152. D. L. Shepelyansky, *Physica D* **28**, 103 (1987).
153. G. Casati, B.V. Chirikov, and D. L. Shepelyansky, *Phys. Rev. Lett.* **53**, 2525 (1984).
154. G. Casati, I. Guarneri, and D. L. Shepelyansky, *IEEE Quant. Electron* **QE-24**, 1420 (1988).
155. G. Casati and L. Molnari, *Progr. Theor. Phys.* **98**, 287 (1989).
156. P. W. Milonni, J. R. Ackerhalt and M. E. Goggin, *Phys. Rev. A* **35**, 1714 (1987).
157. G. M. Zaslavsky, *Phys. Rep.* **80**, 175 (1981).
158. G. P. Berman and A. R. Kolovsky, *Physica D* **8**, 117 (1983).
159. F. Haake, *Quantum Signatures of Chaos*, Springer, Berlin, 1991.
160. L. R. Reichl, *The Transition to Chaos: Quantum Manifestations*, Springer, Berlin, 1992.
161. G. Casati and B.V. Chirikov, *Physica D* **86**, 220 (1995).
162. C. C. Gerry and E. R. Vrscaj, *Phys. Rev. A* **39**, 5717 (1989).
163. G. J. Milburn and C. A. Holms, *Phys. Rev. A* **44**, 4704 (1991).
164. W. Leoński, *Physica A* **233**, 365 (1996).
165. P. Szlachetka, K. Grygiel, and J. Bajer, *Phys. Rev. E* **48**, 101 (1993).
166. K. Grygiel, and P. Szlachetka, *Phys. Rev. E* **51**, 36 (1995).
167. K.N. Alekseev and J. Peřina, *Phys. Rev. E* **57**, 4023 (1998).
168. J. Peřina, *Quantum Statistic of Linear and Nonlinear Optical Phenomena*, Kluwer, Dordrecht, 1991.
169. J. Peřina, J. Křepelka, R. Horák, Z. Hradil, and J. Bajer, *Czech. J. Phys. B* **37**, 1161 (1987).
170. R. Schack and A. Schenzle, *Phys Rev. A* **41**, 3847 (1990).
171. P. Szlachetka, K. Grygiel, J. Bajer, and J. Peřina, *Phys. Rev. A* **46**, 7311 (1992).
172. K. Grygiel, W. Leoński, and P. Szlachetka, *Acta Phys. Slovaca* **48**, 379 (1998).
173. B. Sundaram and P. W. Milonni, *Phys. Rev. E* **51**, 1971 (1995).
174. L. E. Ballentine and S. M. McRae, *Phys. Rev. E* **58**, 1799 (1998).
175. M. Toda and K. Ikeda, *Phys. Lett. A* **124**, 165 (1987).
176. G. J. Milburn *Phys. Rev. A* **33**, 674 (1986).
177. K. Vogel and H. Risken, *Phys. Rev. A* **38**, 2409 (1988).
178. P. D. Drummond, K. J. McNeil, and D. E. Walls, *Optica Acta* **28**, 211 (1981).
179. P. Szlachetka, *J. Phys. A* **20**, 1455 (1987).